Laser Machining of 7075 T6 Aluminium alloy and Effect of Thermal Treatment on Tensile and Hardness

A thesis submitted towards partial fulfillment of the requirements for the degree of

Master of Technology in Laser Science & Technology

Submitted by

PRASHNA MAITY

Examination Roll No: M4LST24003

Registration No: 163804 of 2022-23

Under the guidance of

Dr. Amit Karmakar
Professor
Mechanical Engineering Department
Jadavpur University, Kolkata

Dr. Apurba Das
Assistant Professor
Dept. of Mechanical Engineering
IIEST, Shibpur

School of Laser Science and Engineering
Faculty of Interdisciplinary Studies, Law and Management
Jadavpur University
Kolkata-700032
India
May 2024

M.Tech in Laser Science and Technology
Course affiliated to
Faculty of Engineering and Technology
and offered by
Faculty of Interdisciplinary Studies, Law and Management
Jadavpur University
Kolkata, India

CERTIFICATE OF RECOMMENDATION

This is certified that the thesis entitled **"Laser Machining of 7075 Aluminium alloy and Effect of Thermal Treatment on Tensile and Hardness"** is a bonafide work carried out by **PRASHNA MAITY** under my supervision and guidance for partial fulfillment of the requirement for post graduate degree of **Master of Technology in Laser Science & Technology** in **School of Laser Science and Engineering** during the academic session 2023-2024

……

Thesis Supervisors

Dr. Amit Karmakar
Professor
Department of Mechanical Engineering
Jadavpur University
Kolkata-700032

&

Dr. Apurba Das
Assistant Professor
Dept. of Mechanical Engineering
IIEST, Shibpur-711103

……
Sri. Dipten Misra
Director, School of Laser Science and Engineering
Jadavpur University, Kolkata-700032

……...
Dean
Faculty of Interdisciplinary Studies, Law and Management
Jadavpur University, Kolkata-700032

M.Tech in Laser Science and Technology
Course affiliated to
Faculty of Engineering and Technology
and offered by
Faculty of Interdisciplinary Studies, Law and Management
Jadavpur University
Kolkata, India

CERTIFICATE OF APPROVAL**

This foregoing thesis is hereby approved as a creditable study of an engineering subject carried out and presented in a manner satisfactory to warrant its acceptance as a pre-requisite to the degree for which it has been submitted. It is understood that by this approval the undersigned do not necessarily endorse or approve any statement made, opinion expressed or conclusion drawn therein but approve the thesis only for the purpose for which it has been submitted.

Committee of final examination for evaluation of thesis

……
……
……

**Only in case the recommendation is concurred

DECLARATION OF ORIGINALITY AND COMPLIANCE OF ACADEMIC ETHICS

The author hereby declares that this thesis contains original research work by the undersigned candidate as part of his Master of Technology in Laser Technology studies during academic session 2022-2024.

All information in this document has been obtained and presented in accordance with academic rules and ethical conduct.

The author also declares that as required by the rules and conduct, the author has fully cited and referred all material and results that are not original to this work.

NAME: **PRASHNA MAITY**

EXAMINATION ROLL NO.:**M4LST24003**

THESIS TITLE: **Laser Machining of 7075 T6 Aluminium alloy and Effect of Thermal Treatment on Tensile and Hardness**

SIGNATURE: DATE:

ACKNOWLEDGEMENT

First and foremost, I thank almighty God (Hari Om) for giving me the ability and patience and blessing me with success to complete this thesis.

I would like to gratefully thank my academic supervisors, Prof. Amit Karmakar and Dr. Apurba Das; it is truly a pleasure working under them, for their unlimited support, continuous encouragement and durable patience during my project. Because of their close supervision and great knowledge and professionalism I have experienced a significant event in my life with a positive effect to a promising future.

I would also like to express my deep sense of thankfulness to Sri. Dipten Misra for providing me the proper atmosphere of work.

I would also want to express my gratitude to my lab seniors and research scholars, Sourav Majumdar and Palash Mondal for making this journey a happy and a joyous one.

Finally, special thanks to my parents for encouraging me while I am far away from them & for their patience, time and understanding.

PRASHNA MAITY

Examination Roll No: M4LST24003

Registration No: 163804 of 2022-23

Class Roll No : 002231201006

List of Nomenclatures

Symbol	Description
$[C]$	Matrix of specific heat
$c(T)$	Specific heat as a function of temperature, J/kg. K
E	Young's modulus
$F(t)$	External load vector
$F_{th}(t)$	Vector of temperature load
h	Heat transfer coefficient, W/m^2.K
I_0	Intensity of laser at (0,0), W/cm^2
$[K]$	Matrix of conductivity
$K(T)$	Matrix of temperature dependent stiffness
$k(T)$	Thermal conductivity as a function of temperature, W/m.K
$\{Q\}$	Vector of nodal heat flow
Q_{in}	Heat generation rate, W/m^2.K
R	Surface reflectivity
r	laser beam radius, mm
$\{T\}$	Nodal temperatures vector
$\{\dot{T}\}$	Vector of Time derivative of $\{T\}$
T_{ext}	External temperature, K
$\{u(t)\}$	Vector of displacement
x, y	Distance from centre (0,0) of the laser beam in x and y direction, m
α	Thermal expansion coefficient
υ	Poisson's ratio
ρ	Density of material, kg/cm^3

List of figures

List of tables

Table of Contents

Chapter 1

Introduction

1.1 Background

7075 Aluminium alloy was developed over 70 years ago. However, many researches still have been performed on it in the past decade [1–2]. High strength and light weight properties of the alloy are attractive properties leading to its prevalent usage in transport applications corresponding to constantly increasing global warming concerns. In addition, 7075 Al alloy is being put into lightweight components and are being applied in aviation, energy and even in the medical field [3].

1.2 Aluminium 7075 T6 alloy

Aluminium alloys are the second most used metallic alloy materials as a structural material, after steel. Various parts from automobile industry are manufactured by aluminium alloys including air frames, engines, and satellite components. Aluminum and its alloys are employed in a wide range of wrought and cast forms, as well as heat treatment conditions. Due to its special combination of characteristics, which make it one of the most adaptable building and industrial materials, aluminum is becoming more and more in demand. Heat treatments and alloying ingredients give aluminum its ideal characteristics. This encourages the production of small hard precipitates that impede the movement of dislocations and enhance the material's mechanical characteristics, including strength and hardness [4-14]. Chemical compositions of 7075 Aluminium Alloy are given in Table 1 and some applications of Al 7075 alloy are shown in Fig. 1.

The airplane industry frequently uses 7075 Al alloy for its comprehensive qualities, including low density (2.7 g/cm^3), high strength, ductility, toughness, and fatigue resistance, in the structural components of the fuselage [15]. The main alloying elements that give the materials their increased strength, toughness, and hardness are magnesium (Mg) and zinc (Zn). According to Staley's research [16], the 7xxx series alloys contain three different kinds of particles:

component particles, dispersoid particles, and fine-strengthening precipitate particles. Because of the fine precipitates, such as $Al_2Mg_3Zn_3$ and $MgZn_2$, the alloys in the 7xxx series have a high strength. The dispersoid particles, which are soluble exclusively in liquid and include $Al_{12}Mg_2Cr$ and $Al_{18}Mg_3Cr_2$, may be crucial in maintaining grain and subgrain boundaries and preventing the alloys from recrystallizing. $MgZn_2$ precipitates predominate in the T6 temper. With a size range of 2–5 nm, they are homogeneously dispersed [13]. By comparing the precipitate spots to the diffraction patterns of precipitates in other Al–Zn– Mg(–Cu) alloys, Du et al. [17] revealed that the precipitates spots are mostly from η′ (metastable $MgZn_2$) and a tiny amount of stable η ($MgZn_2$).

Table 1 : Chemical composition of 7075 Aluminium Alloy [16]

Elements	In %
Si	Max 0.40
Fe	Max 0.50
Cu	1.2-2.0
Mn	Max 0.30
Mg	2.1-2.9
Cr	0.18-0.28
Zn	5.1-6.1
Ti	Max 0.20
Others Each	Max 0.05
Others Total	Max 0.15
Al	87.1-91.4

(a)

(b)

Fig. 1: (a) 7075 Forging components of machine components, and (b) 7075 Aluminum Wire, High-strength Alluminum Wire, Cold Heading Wire

As 7075 aluminium is heat-treatable, it can be possible to improve its mechanical properties (hardness & tensile strength) with proper heat treatment process. Three steps make up the 7075 aluminum heat treatment process: solution heat treatment, quenching and age hardening. The T6 temper identification code is one of the heat treatments applied to 7075 aluminum. The T6 treatment procedure was conducted between 465°C and 490°C for the solution heat treatment and 120°C for the aging temperature [18].According to Li, J.F. et al. [11], T6 was subjected to a temperature range of 450–480°C for solution heat treatment and 120–185°C for aging, Concurrently, Y. Mahathaninwong, N. et al. [19] studied the material used in 7075 aluminum castings made using rheocasting methods in a similar manner. The formation of $MgZn_2$ and Al_2CuMg is the cause of the enhancement in mechanical characteristics of 7075 aluminum [11,19,20]. The goal of this study was to determine the ideal temperature for age hardening to improve the hardness and tensile strength of 7075 aluminum by the application of the T6 temper treatment.

1.3 Laser Cutting of Al 7075 T6 alloy

Aluminium and its alloys are the most versatile and acceptable engineering materials because of their unique characteristics such as high strength-to-weight ratio, more resistance to corrosion, high thermal and electrical conductivity, non-toxicity and ease of formability & machinability. There are specific applications of recently developed Al 7075 alloys; like aircraft fittings, aerospace, missile parts, defense equipments, etc. Machining of complex shapes with minimum feature size and finishing standard of these alloys is found to be difficult using conventional machining processes.

1.4 Thermal treatment Al 7075 T6 alloy

Many researches still have been performed on it in the past decade [1-6], High strength and light weight properties of the alloy are attractive properties leading to its prevalent usage in transport applications corresponding to constantly increasing global warming concerns. In addition, 7075 Al alloy is being put into lightweight components of lower limb prostheses [12]. 7075 Aluminium alloy was commonly formed by wrought manufacturing process which resulted in high strength. However, the cost of this production route is very high compared to the alternative

casting route. Nevertheless, disadvantages of conventional casting are found in the material structure with existence of casting defects such as pores and shrinkage cavities, including lower strength [1,21].

1.5 Objectives of the study

a) Modeling of the laser cutting of Al 7075 T6 alloy.
b) Determination of the stress distribution and HAZ for the laser cutting.
c) Thermal treatment of the Al 7075 T6 alloy at different aging temperature and holding time.
d) Determination the effect of Thermal treatment on ultimate strength property of the Al 7075 T6 alloy.
e) Determination the effect of Thermal treatment on hardness property of the Al 7075 T6 alloy.

1.6 Organization of the thesis

This thesis starts with the introduction section, elaborating the background of research and stating the objectives of the present study in Chapter 1.

It is then followed by literature survey to present associated theory, methods and findings of past research in Chapter 2.

Chapter 3 gives details of the material and methodology implemented in the process considered in this work. Modeling of the laser cutting of Al 7075 T6 alloy and thermal treatment process.

Chapter 4 portrays the results and discussion of the laser cutting simulation and thermal treatment effect.

Chapter 5 deals with Microscopic study of the Al 7075 T6 alloy. Finally,concluding with future scope of the present work are presented in Chapter 6.

Chapter 2

Literature Survey

2.1 7075 Aluminium alloy

7075 Aluminium alloy was commonly formed by wrought manufacturing process which resulted in high strength. However, the cost of this production route is very high compared to the alternative casting route. Nevertheless, disadvantages of conventional casting are found in the material structure with existence of casting defects such as pores and shrinkage cavities, including lower strength [1,21]. An alternative Semi-Solid Metal (SSM) process was developed in early 1971 [22]. Reduction in casting temperature and solidification shrinkage is its main advantage [23]. This SSM process has since been developed into thixocasting and rheocasting processes. Rheocasting process has increasingly gained attentions from many researchers because of less investment and lower raw material cost compared to thixocasting process. Hence, rheocasting process will be the alternative process to obtain higher strength alloys than cast alloy requirements. Various techniques for semisolid slurry preparations of 7075 Al alloy had been proposed such as cooling slope [3], induction stirring with simultaneous forced air cooling [24], and a novel technique of rheocasting process developed by the Innovative Metal Technology (IMT) teamof the Prince of Songkla University. This technique is called Gas Induced Semi-Solid (GISS) technique [12]. It is a simple, economical and efficient process. Additionally, this technique has succeeded to produce non-dendritic structure of 7075 alloy. However, in order to obtain high strength 7075 Al alloy, heat treatment is a key process to improve mechanical properties after the forming process. T6 heat treatment is one of the major factors to enhance mechanical properties of the alloy through an optimization of both the solution heat treatment and the artificial aging conditions applied to the alloy [5,25]. T6 heat treatment schedule of wrought 7075 Al alloy were well established at the solution temperature range of 465–490 ◦C and aging temperature of 120˚C [18]. In contrast, dissolving soluble phases of the as-cast 7075 Al alloy should be done at temperature lower than 465 ◦C as advised by Mukhopadhyay [26]. Moreover, various aging times at 120˚C for7075 Al alloy have been proposed to be the peak-aged condition ofT6 heat treatment [10, 11]. As the difference in as-fabricated microstructures led to the differences in solution heat treatment and artificial aging conditions, this work hence

aims to establish T6 heat treatment data of the 7075 Al alloy produced by rheocasting process along with a GISS technique. This is focused into two main sections of T6heat treatment; solution heat treatment and artificial aging. The influence of solution heat treatment and artificial aging temperature and time on mechanical properties and microstructures was investigated. A brief overview of different Al alloy used in specific applications is shown in the Fig. 2.

Fig. 2: A brief overview of different Al alloy used in specific applications

2.2 Application of Aluminium 7075 alloy

Technological developments across all fields and especially in the material science field is considered as a thriving research frontier in the contemporary development of lightweight materials such as composite materials [27,28]. By 2025, the U.S. automotive industry hopes to achieve a corporate average fuel economy rating of 54.5 miles per gallon (mpg), this is much higher than 2016's requirement of 35.5 mpg [29]. In this regard, lightweight materials such as composite materials hold great promise. Even though they are commercialized after the 2nd world War but composite materials are old as our human civilization [30]. They are formed by two or more different materials for achieving higher physical and mechanical properties in comparison to the

individual materials to meet industrial needs and the demand of modern engineering applications [31]. Being the third most abundantly available element in the earth's crust, aluminium metal and its various alloys are widely used for various emerging applications such as automobile and aircraft structures. Particularly in the last two decades aluminium metal and its various alloys diverted researchers towards combining innovative structures and new manufacturing routes to develop metal matrix composites (MMCs) [32,33]. The role of MMC in developing aircraft structures is highly promising due to their higher mechanical properties, low weight, tailor to design for different requirements, ability to accommodate various other novel nanomaterials, and provide strong potential to evade the strength-ductility trade-off [34]. For high fuel efficiency, weight was reduced and superior-strength composite materials were introduced in the aerospace field [35]. Among these criteria for the manufacturing sector, the maximum efficiency and minimum cost of manufacturing routes are considered global competitiveness in product development [36]. Recently, increasing attention has been paid to MMCs due to outstanding mechanical strength, and good wear resistance [37]. Currently, popular matrix materials are aluminium, magnesium, and titanium. But according to reports Aluminium-based MMCs (AMMCs) are accounted for about 69% of mass annually for various industrial uses such as aviation, automobiles, electronic devices, marine industries and space shuttles [38]. AMMC offers a wide range of remarkable physical, and mechanical properties and their combination of properties such as improved ductility, toughness, formability, and electric and thermal conductivities. Fig. 3 shows the application of Al alloy in aviation where 7075 Alloy is mainly used in wings. The applications of Al 7075 alloy in different industries are portrayed in Fig. 4.

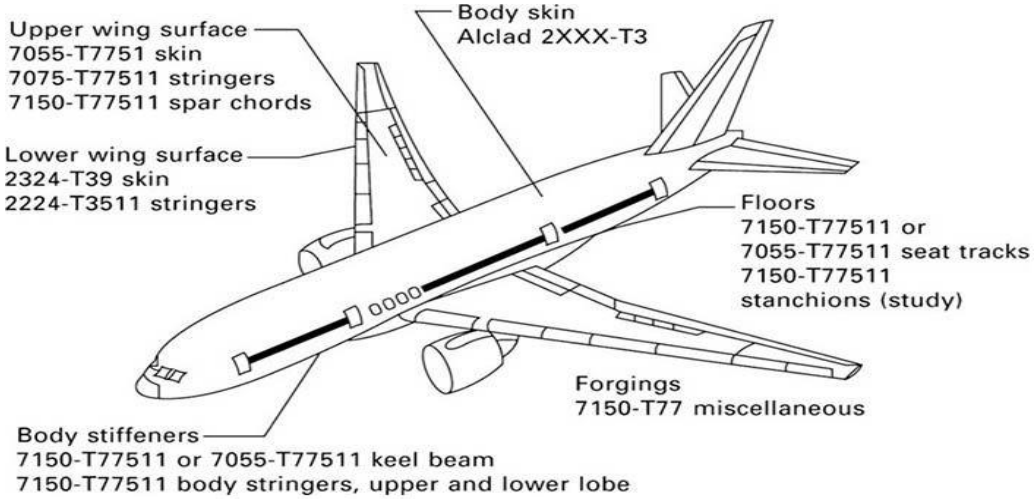

Fig. 3: Application of Al alloy in aviation. 7075 is mainly used in wings

Fig. 4: Application of Al 7075 alloy in different industries

2.3 Laser cutting of Aluminium 7075 alloy

Applications of laser beam in modern industries are increasing at a fast pace due to their ability to cut very hard as well as soft materials, electrically conductive as well as non-conductive materials, such as HSS, super alloys, ceramics, composites, diamond, plastics and rubber [39]. One of the main objectives of laser machining is to observe and minimize the HAZ. Arau´ jo et al. [40] observed heat affected zone (HAZ) extension in CO2 laser cutting of 2024 aluminum alloy. Stournaras et al. [41] investigated experimentally the quality of laser cutting for the aluminum alloy AA5083 of 2 mm thickness with the use of a pulsed CO2 1.8 kW laser. The quality of the cut has been monitored by measuring kerf width, edge roughness and size of the HAZ by evaluating laser power, scanning speed, frequency and gas pressure. Dubey et al. [42] optimized two kerf qualities such as kerf deviation and kerf width simultaneously using Taguchi quality loss function during pulsed Nd:YAG laser beam cutting of aluminium alloy sheet of 0.9 mm-thick. Sharma et al. [43] presented the modeling and optimization of cut quality characteristics i.e. kerf deviation (Da) and kerf taper (Ta) during Nd:YAG laser cutting of aluminum alloy thin sheet along the curved profile. The input process parameters are identified as arc radius of curve profile, oxygen pressure, pulse width, pulse frequency and cutting speed. Riveiro et al. [44] observed influence of processing parameters and optimal conditions of edge surface aspect, dross characteristics and HAZ for CO_2 laser cutting of aluminium–copper alloy (2024-T3). Laser processing is suitable for geometrically

complex profile cutting, drilling, marking and making miniature holes. Kardas et al. [45] carried out experimental investigation on laser cutting of rectangular geometry in 2024 aluminum sheet under high pressure nitrogen assisting gas to investigate temperature and thermal stress fields. Yilbas et al. [46,47] carried out laser cutting of a triangular geometry into aluminum 2024 alloy for analyzing thermal stress field. Leone et al. [48] investigated experimentally the kerf geometry laser in cutting of 6061-T6 aluminium alloy sheets by means of a 150 W multimode pulsed Nd:YAG laser. Sharma et al. [49] presented modeling and optimization of cut quality in terms of kerf taper (Ta) and surface roughness (Ra) during pulsed Nd:YAG laser cutting of thin Al-alloy sheet for straight profile. Laser cutted Al 7075 parts for industrial use are shown in Fig. 5.

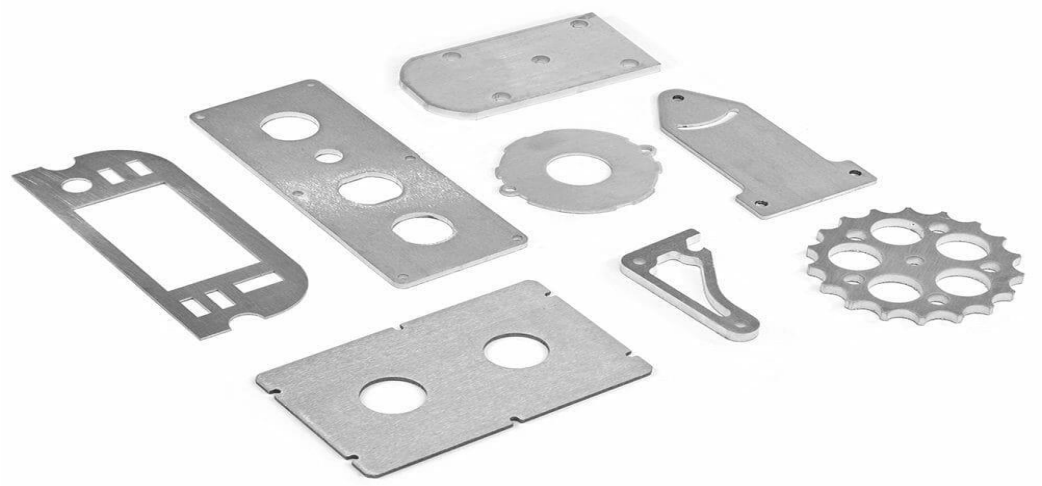

Fig. 5: Laser cutter Al 7075 parts for industrial use.

2.3 Thermal treatment Al 7075 T6 alloy

An alternative Semi-Solid Metal (SSM) process was developed in early 1971 [22]. Reduction in casting temperature and solidification shrinkage is its main advantage [23]. This SSM process has since been developed into thixocasting and rheocasting processes. Rheocasting process has increasingly gained attentions from many researchers because of less investment and lower raw material cost compared to thixocasting process. Hence, rheocasting process will be the alternative process to obtain higher strength alloys than cast alloy requirements. Various techniques for semisolid slurry preparations of 7075 Al alloy had been proposed such as cooling slope [3], induction stirring with simultaneous forced air cooling [24], and a novel technique of rheocasting process developed by the Innovative Metal Technology (IMT) team of the Prince of Songkla

University. This technique is called Gas Induced Semi-Solid (GISS) technique [12]. It is a simple, economical and efficient process. Additionally, this technique has succeeded to produce non-dendritic structure of 7075 alloy. However, in order to obtain high strength 7075 Al alloy, heat treatment is a key process to improve mechanical properties after the forming process. T6 heat treatment is one of the major factors to enhance mechanical properties of the alloy through an optimization of both the solution heat treatment and the artificial aging conditions applied to the alloy [5,25]. T6 heat treatment schedule of wrought 7075 Al alloy were well established at the solution temperature range of 465–490°C and aging temperature of 120 °C [18]. In contrast, dissolving soluble phases of the as-cast 7075 Al alloy should be done at temperature lower than 465°C as advised by Mukhopadhyay [26]. Moreover, various aging times at 120°C for 7075 Al alloy have been proposed to be the peak-aged condition of T6 heat treatment [10,11].As the difference in as-fabricated microstructures led to the differences in solution heat treatment and artificial aging conditions, this work hence aims to establish T6 heat treatment data of the 7075 Al alloy produced by rheocasting process along with a GISS technique. This is focused into two main sections of T6 heat treatment; solution heat treatment and artificial aging. The influence of solution heat treatment and artificial aging temperature and time on mechanical properties and microstructures was investigated.

Chapter 3

Material and Methodology

3.1 Modelling of laser cutting of Aluminium 7075 alloy

When high power laser beam is concentrated on the work piece, the substance of the work piece will absorb some of the high power laser beam's energy and reflect the remaining portion. The part of the laser energy that is absorbed is transmitted into the work piece material and then removed from its surface by the convention effect. Numerous variables, such as the workpiece's composition, polarization, wavelength of the laser beam, optical and thermal characteristics, and so on, affect how well a material absorbs laser energy. It was thus presumed that the substance being employed was opaque and isotropic. When analyzing the laser cutting process, the following presumptions were made:

- The distribution of the laser beam introduced using the Gaussian mode.
- The assist gas pressure utilized to remove the molten material instantly from the workpiece has a minor vaporization effect.
- The thermal history of the heat-affected zone is predicted using convection, conduction and radiation heat transfer, with the assumption that the convection heat transfer coefficient between the workpiece and the environment is constant.
- The cooling effect of assistant gas is ignored.

Modelling of workpiece was performed by using AutoCAD 2021 software. A cuboid with dimensions 20 mm length, 16.5 mm width, and 2 mm height was adopted and modelled as the workpiece, as shown in Fig. 6. The modelling process included specialization of scanning zone by generating tiny cuboids (2 mm length × 0.5 mm width × 2 mm high) along scanning axis as simulation requirements and for adjusting the mesh in the scanning area. The mechanical properties of 7075-T6 Aluminium alloy are given in Table 2.

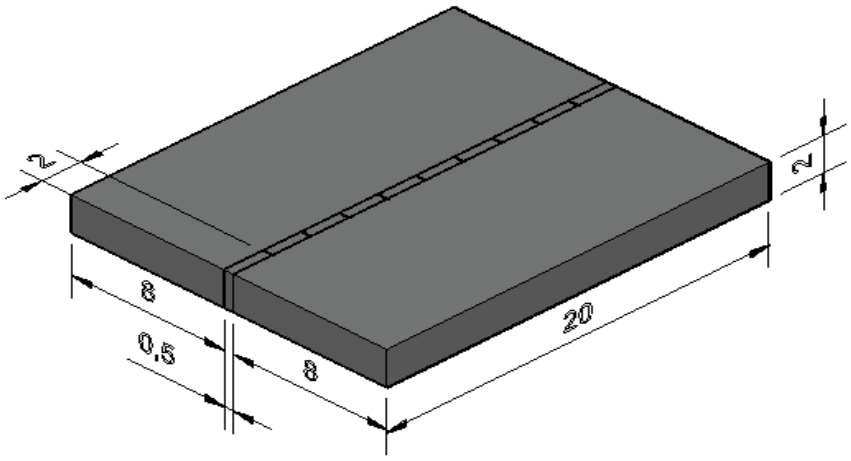

Fig. 6 : Three dimensional model of workpiece of Al 7075 material for analysis

Table 2 : Mechanical Properties of Al 7075-T6 alloy

Sl No.	Parameter	Value	Unit
1	Density	2.81	gm/cc
2	Modulus of Elasticity	71.7	GPa
3	Poisson's ratio	0.33	-
4	Tensile Yield Strength	563 (for sample 'O',i.e. age hardening time is 5Hr), 598 (for sample 'W',i.e. age hardening time is 10Hr)	MPa
5	Ultimate Tensile Strength	610 (for sample 'O',i.e. age hardening time is 5Hr) 630 (for sample 'W',i.e. age hardening time is 10Hr)	MPa
6	Thermal Conductivity	130 (at 77° F)	W/mK
7	Thermal Expansion Coefficient	2.3E-05	/°C
8	Specific heat	960	J/Kg °C
9	Isotropic resistivity	5.15E-06	Ohm-cm

A mesh that divides the computational region into finite elements sizes to facilitate and improve the accuracy of the analysis process. A structured grid with a hexahedral element has been used in

this study. The main features that set structured grids apart from unstructured ones are their higher resolution and superior convergence. As seen in Fig. 7, a refining technique was used in the scanning region exposed to the laser heat flow in order to produce good and precise numerical results.

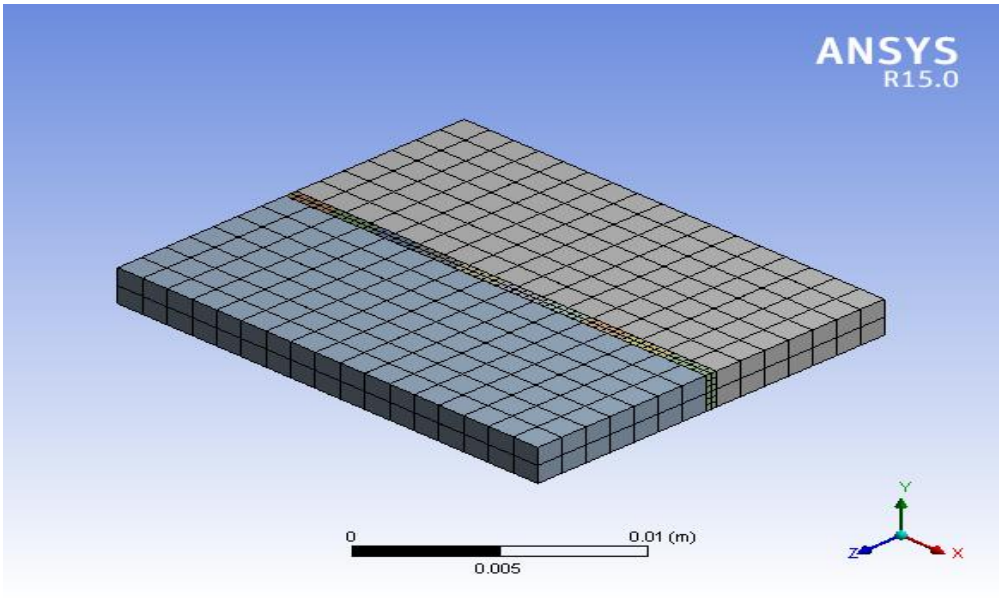

Fig. 7: Three-dimensional model of workpiece after meshing process.

3.2 Governing equation and temperature distribution

The most important aspect of the analysis of laser cutting technology is the modeling of a laser as a heat source. View various beam shapes, such as rectangular, circular, Gaussian, etc., using the beam shaping method. When modeling the laser cutting procedure, the preferred mode is taken into consideration by the Gaussian energy distribution. This is mostly because of the laser's capacity to adjust beam diameter for cutting and energy concentration by producing a high power beam [50].

The intensity of the laser beam that is incident on the material surface can be expressed according to the following equation [51].

$$I_{(x,y,z,t)} = (1-R)I_0^{(-\alpha,z)\left[-\frac{\left(x^2+y^2\right)}{r^2}\right]} \quad (1)$$

Using two-dimensional transients, the heat transport phenomena during laser cutting was simulated. The spatial and temporal temperature distribution T(x,y,t) can satisfy the differential equation for heat conduction in the domain with two dimensions [52]. The governing equation for heat conduction model based on Fourier law can be described below.

$$\frac{\partial}{\partial x}\left[k(T)\frac{\partial T}{\partial x}\right]+\frac{\partial}{\partial y}\left[k(T)\frac{\partial T}{\partial y}\right]+Q_{\text{int}} = \rho c(T)\frac{\partial T}{\partial t} \quad (2)$$

It is essential to specify the boundary and initial conditions of the domain to specify the flow variables on physical field boundaries is readily specified. To solve the governing equations, the boundary and initial conditions should be set as follows;

According to initial conditions: -

- $T_{(x,y.o)} = T_0$ for $(x, y) \in \mathrm{D}$
- $T_{(0,y,t)} = T$
- S_1 for $(0, y) \in S_1$ when $t > 0$, (this condition describe nodal temperatures at flow inlet section, where S_1 symbolizes the inlet surface).

According to boundary conditions:

- $Q_0 = h.(T_{ex} - T)$
- S_2 for $(x, y) \in S_2$ when $t > 0$, (where S_2 symbolizes the surfaces that are exposed to convection and heat fluxes).

Because of the high laser power, the heat scanning zone is created when the laser beam passes over the aluminum alloy surface sheet. Because of the radial conduction and convection activity occurring, such a heat zone will gradually cool. Thermal stresses will consequently arise.

The thermal stresses resulting from temperature difference ΔT can be written as follows: -

$$\sigma_{thermal} = \frac{E\alpha\Delta T}{1-\upsilon} \quad (3)$$

The equivalent stress of Von-misses can be found according to the following equation

$$\sigma_m = \sqrt{\frac{(\sigma_1 - \sigma_2)^2 + (\sigma_2 - \sigma_3)^2 + (\sigma_3 - \sigma_1)^2}{2}} \quad (4)$$

where σ1, σ2, σ3 are the principal stresses for any point in three-dimensional axis (x, y, z).

In the context of laser cutting analysis, temperature is regarded as a dependent variable that influences both mechanical and thermal characteristics. Table 3 lists the parameters that were employed, such as laser power, absorption coefficient, beam radius, etc.

The thermal analysis equations can be obtained using the formulation of finite elements [51]: -

$$\left[C(T)\right]\left\{\dot{T}\right\} + \left[K(T)\right]\{T\} + \{V\} = \{Q(T)\} \quad (5)$$

The mechanical analysis equation can be obtained using the formulation of finite element as:-

$$\left[K(T)\right]\{u(t)\} + \{F(t)\} + \{F_{th}(t)\} = 0 \quad (5)$$

Table 3. Laser cutting parameters selected for analysis.

Sl No.	Parameter	Numerical Values	Unit
1	Laser power	200	W
2	Absorption coefficient	0.15	1/cm
3	Beam radius	0.5	mm
6	Convection heat transfer coefficient	7 (at temperature 22˚C)	W/m^2 ˚C
7	Emissivity	0.7	-
8	Pulse duration	2	ms
9	Pulse frequency	28	Hz

As seen in Fig. 8, the simulation procedure was carried out using the cutting settings indicated in Table 3. Along the aluminum alloy workpiece's symmetrical axis, or "X-axis," the laser beam advances. The mechanical deformation resulting from laser cutting heat flow was considered insignificant in the current investigation.

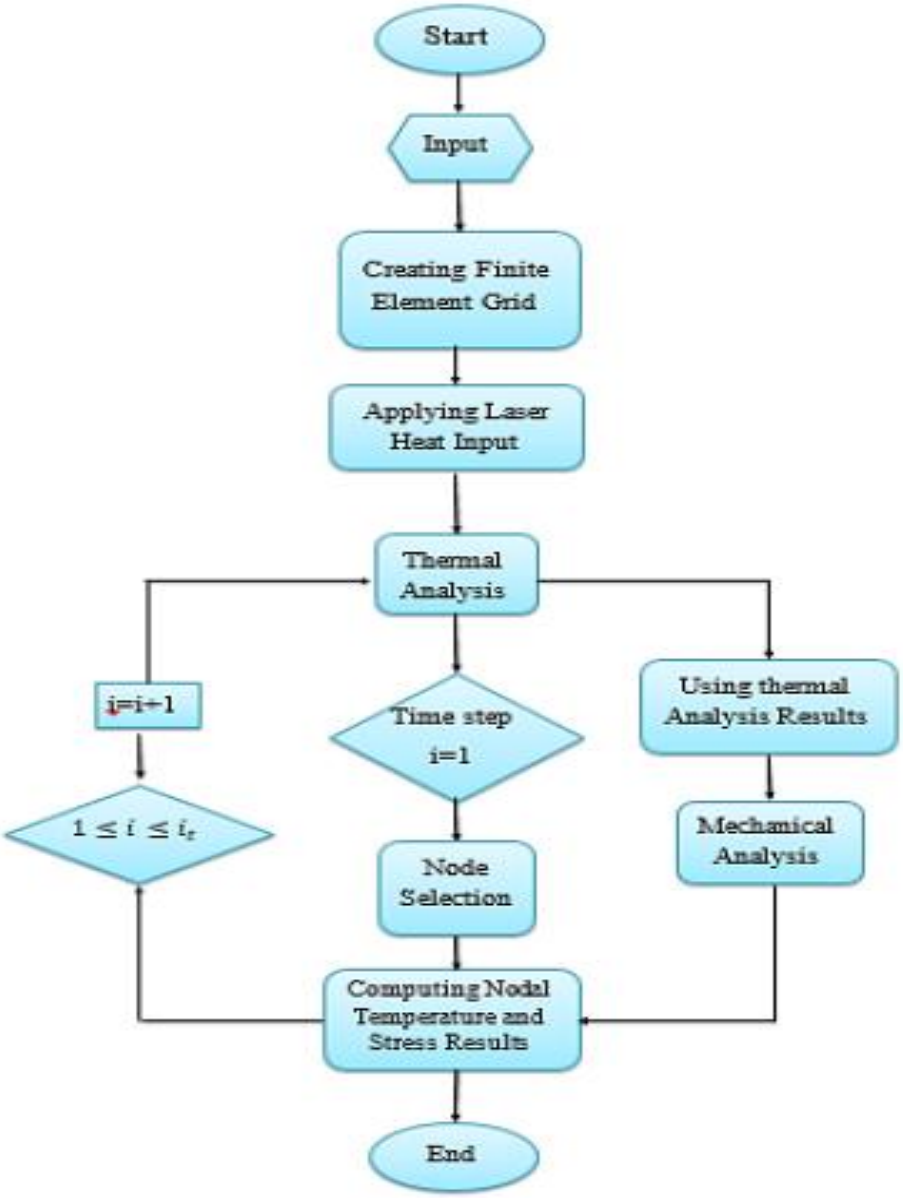

Fig. 8: Flow chart illustrates the simulation process.

ANSYS software was utilized to conduct an analysis that included coupled physics in order to look at the temperature distribution and subsequent thermal stress. Using the APDL programming language, "ANSYS Parameter Design Language," the mechanical analysis uses the thermal analysis's output data as input data.

3.3 Thermal treatment process

Two stage of heat treatments were carried out on the Muffle Furnace. The specimens ID (A, E, I, O, U, W) subjected to T6 heat treatment process consists of materials were carried out at 480°C, soaking them at this temperature 60 minutes. The Time vs Temperature graph of a T6 treatment show in Fig. 9 Then quenched in ice cool water. Muffle furnace used for heat treatment .

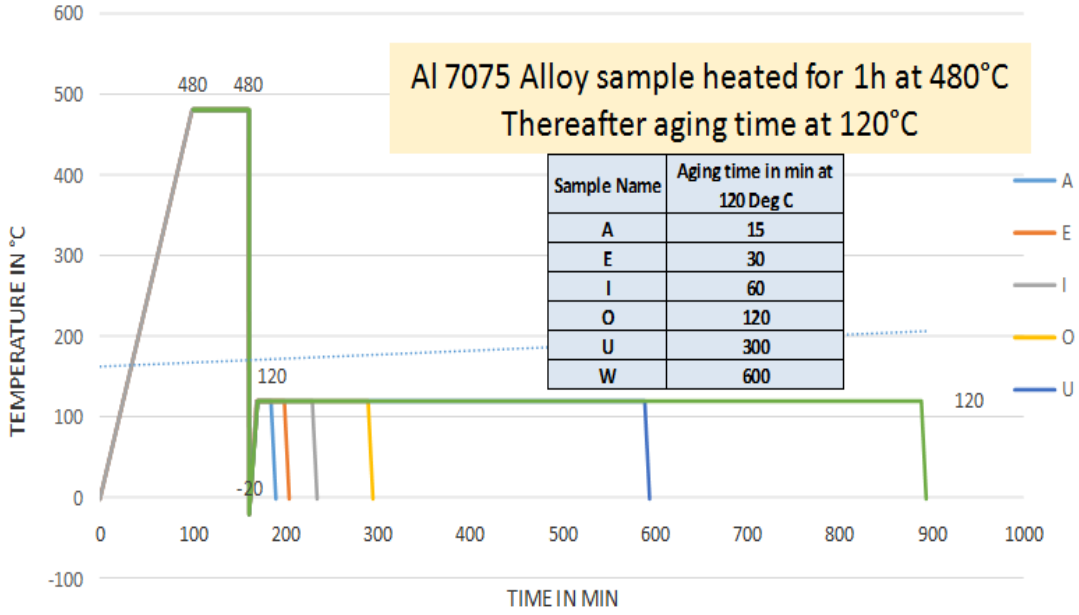

Fig. 9: Heat Treatment temperature plot with holding and aging time

Table 4 : Technical Specification of Muffle Furnace

Parameter	Value
Max Temperature	1100°C
Continuous Operating Temperature	1000°C
Heating Element	KANTHAL A1 wire
Heating Chamber MOC	Ceramic board
Thermocouple	K Type
Temperature Controller	Programmable PID Controller (Ramp & Dwell)
Power Supply	220V/50Hz
Door	Swing type insulated solid door

Fig. 10: Tenney chember used for again heat treatment (-70°C to 200°C)

3.4 Aging temperature and holding time

Subsequently the quenched specimens were subjected to aging at 120°C, soaking them at this temperature specimens (A at 15 minutes, E at 30 minutes, I at 60 minutes, O at 120 minutes, U at 300 minutes, W at 600 minutes,) by air cooling at room temperature. The tenney chember used for this cycle. The marked samples are shown in Fig. 11.

Sample Name	Again Heat Treatment Time
A	15 Min
E	30 Min
I	60 Min
O	120 Min
U	300 Min
W	600Min

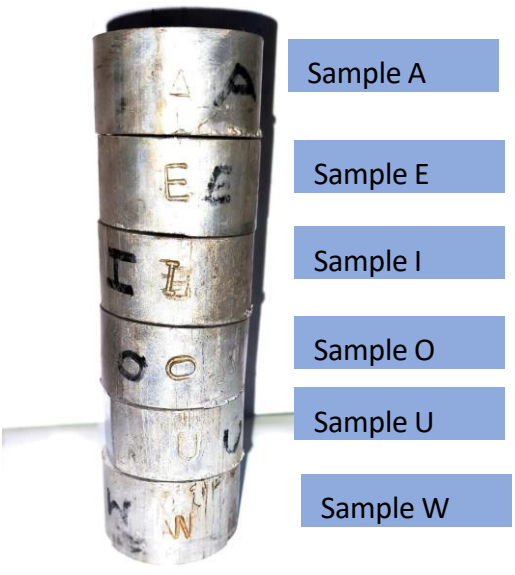

Fig. 11: Again Heat Treatment Sample

Chapter 4

Study of Simulation and Thermal treatment effect

4.1 Temperature distribution from Laser cutting analysis

Figures 12 and 13 illustrate the temperature distribution contours after pass 1- and 10-seconds heat duration respectively. The irradiated line of laser match to the straight line when y=0, the maximum heating loads are constantly at this straight line during the heating process.

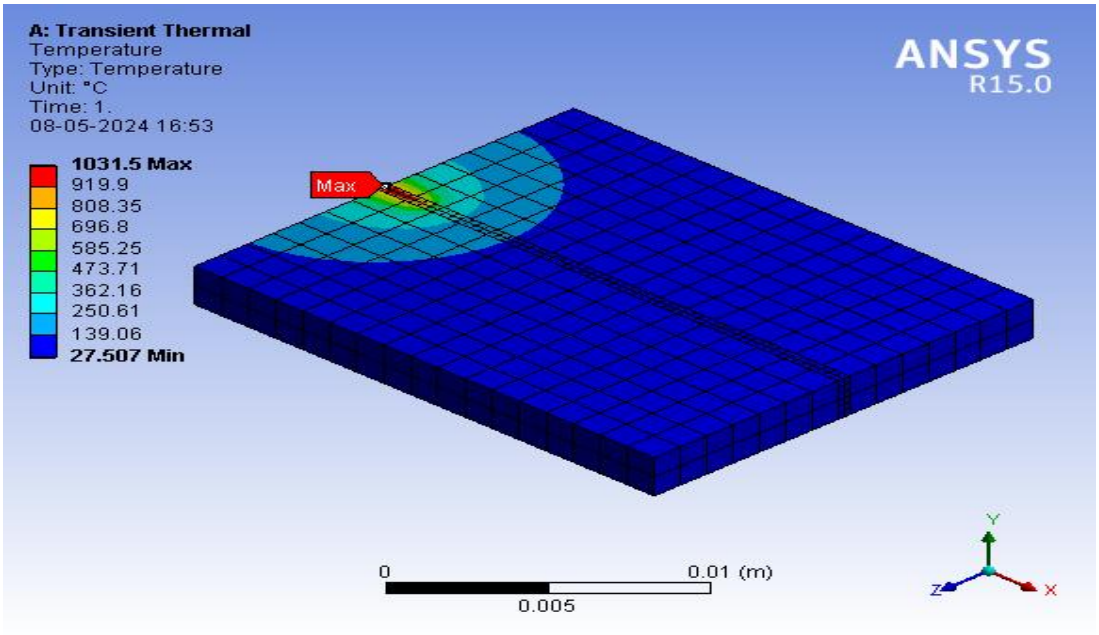

Fig. 12: Temperature distribution contour at t=1 s

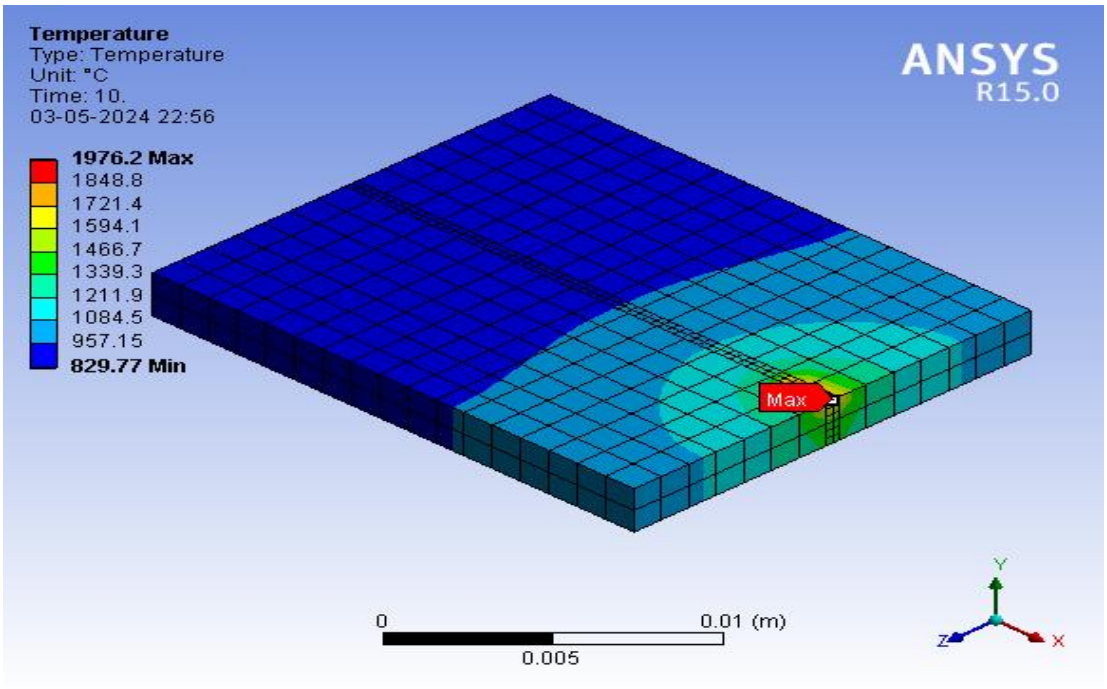

Fig. 13: Temperature distribution contour at t=10 s

The above figures indicate that the greatest temperature is detected on the workpiece where the center of the laser-focused spot is located. The temperature approaches the "melting temperature" of the material at the laser center spot because the laser's highest intensity is concentrated there. The outcome will be a notable variation in temperature between the frontal neighborhood locations and the point temperature located in the center of the beam. A good and continuous cutting process will be aided by the laser's continuous scanning speed and the preheating action caused by heat transfer between the workpiece's frontal regions and concentrating point [47]. The temperature distribution of the Al 7075 T6 aluminum alloy workpiece is shown in a longitudinal cross section contour in Figures 14 and 15. The high thermal conductivity of the aluminum alloy is considered to be the reason for the apparent increase in temperature behind the laser beam spot along the surface during the cutting process.

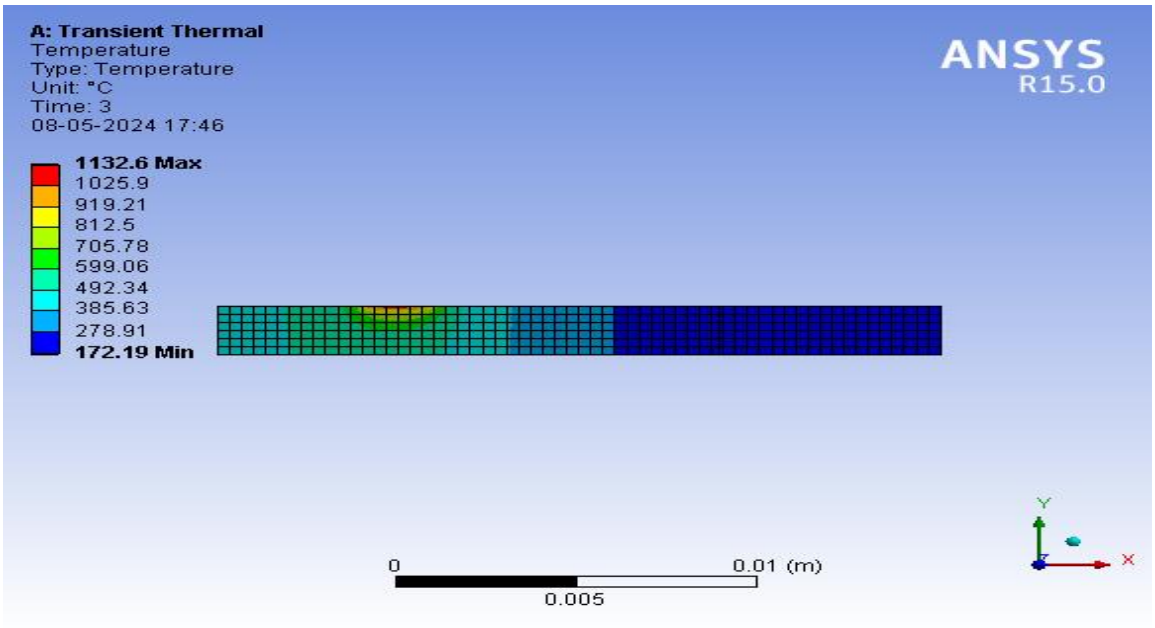

Fig. 14: Longitudinal cross-section contour of temperature distribution at t=3 s.

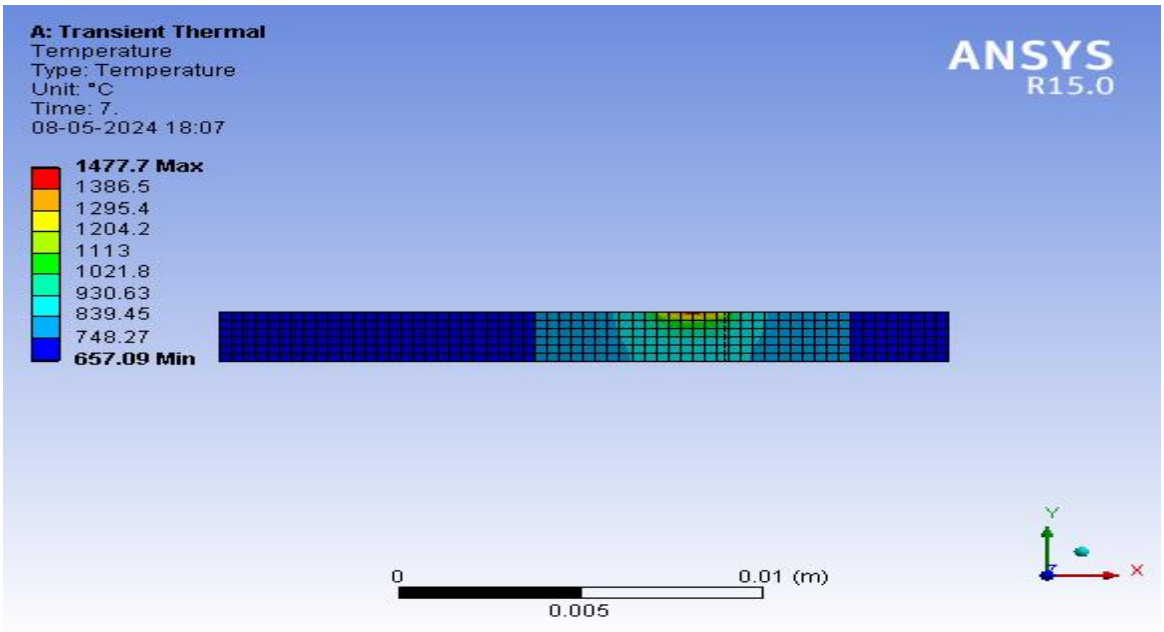

Fig. 15: Longitudinal cross-section contour of temperature distribution at t=7 s.

Figure 16 represents the variation of temperature of Al 7075 T6 workpiece during laser cutting process. It also indicates that cutting zone temperature gradually increases with time which is believed to be due to the high thermal conductivity of aluminium alloy. As a result, the heat of

conduction will increase from heated region to the solid bulk. Since aluminium thermal conductivity is proportional to its temperature [51], causing high-thermal gradients at the surface of workpiece. Ambient temperature is also increased due to high convection coefficient which is also responsible for increasing the cutting zone temperature and maximum heat affected zone (HAZ) is depicted in Fig. 13.

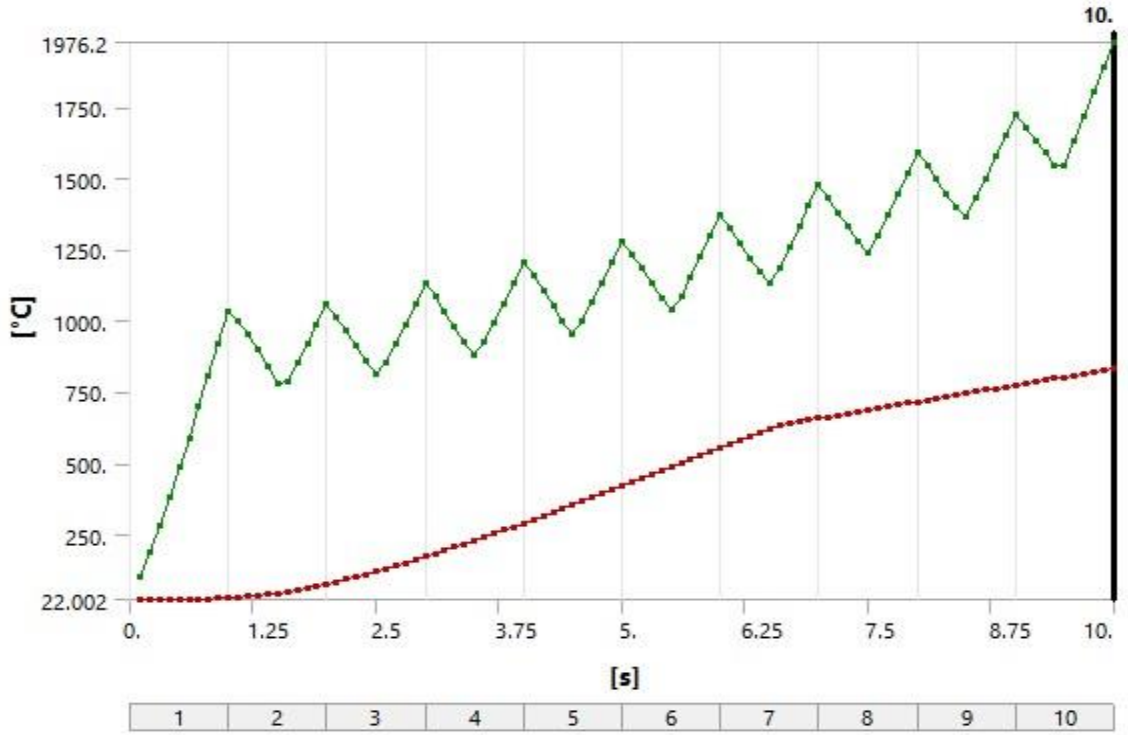

Fig. 16: Temperature variation during the laser cutting process (Green color line indicates cutting zone temperature and red color line indicates ambient temperature)

4.2 Stress distribution from Laser cutting analysis

Figures 17 and 18 show distribution contours of Von Mises-stress along the surface of the workpiece at a certain time step for sample ‘O’ (i.e. age hardening time is 5Hr) and sample ‘W’ (i.e. age hardening time is 10(Hr) respectively. Both Figures indicate that the regions located along the scanning line of the workpiece surface where they affected by the focused laser beam achieved high values of von Mises stress. It can be concluded from the figures that maximum Von-Mises stress is observed for sample ‘O’.

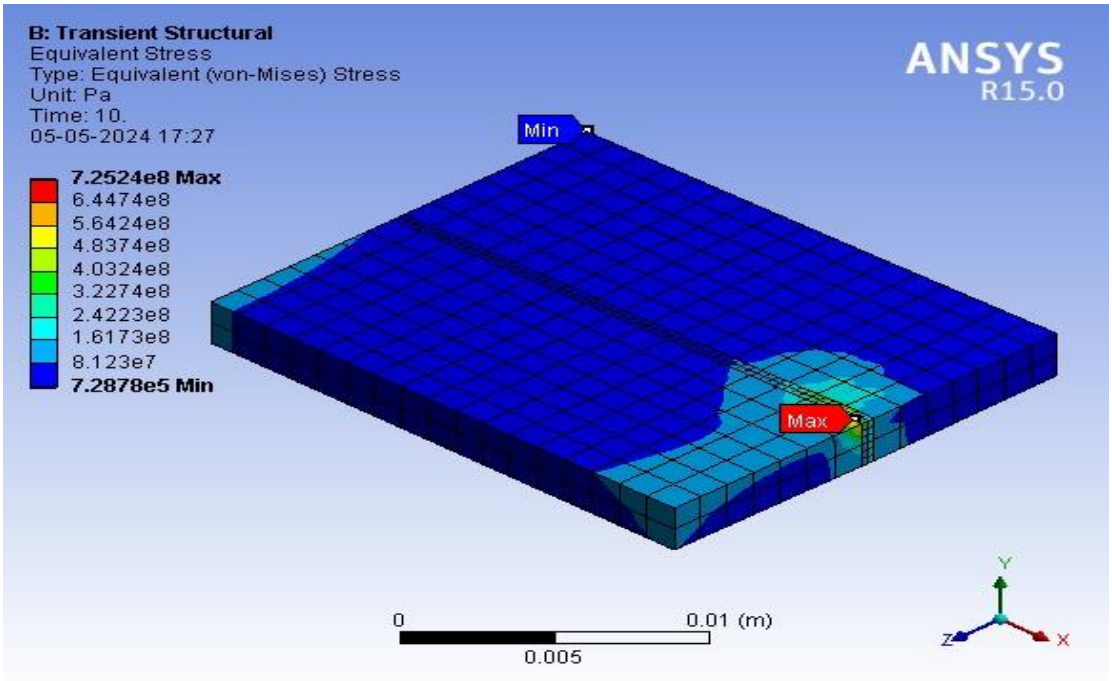

Fig. 17: Distribution contour of equivalent (Von-Mises) stress at t=10 sec (for sample 'O',i.e. age hardening time is 5Hr)

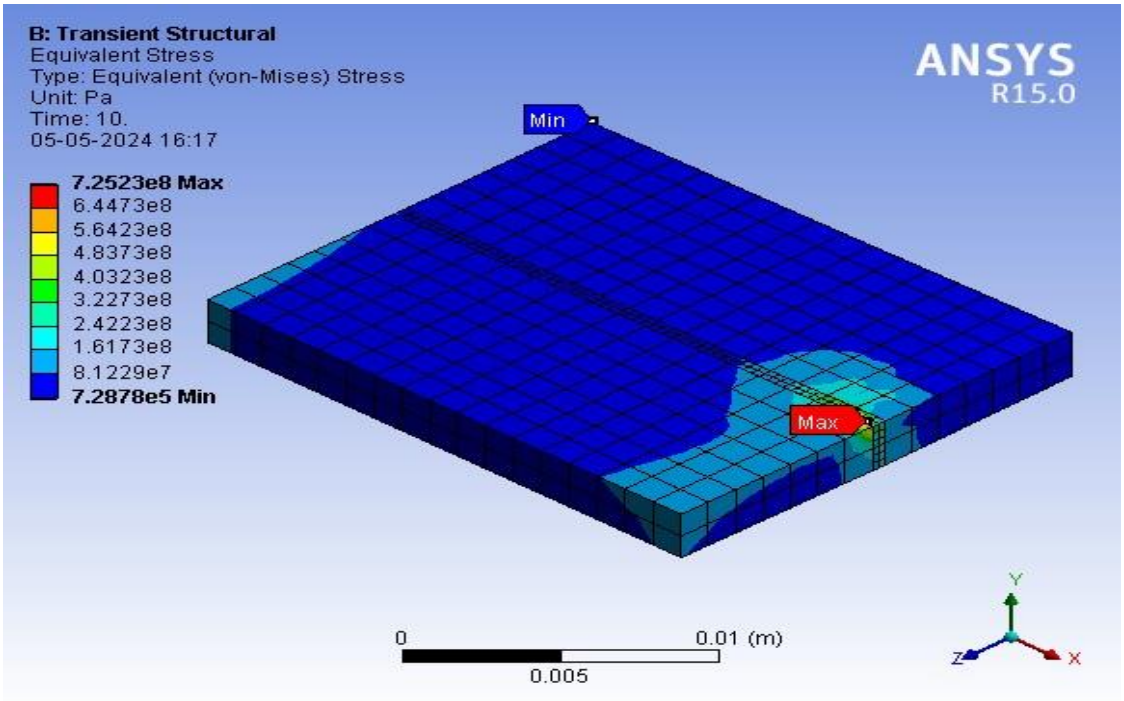

Fig. 18: Distribution contour of equivalent (Von-Mises) stress at t=10 sec (for sample 'W',i.e. age hardening time is 10Hr)

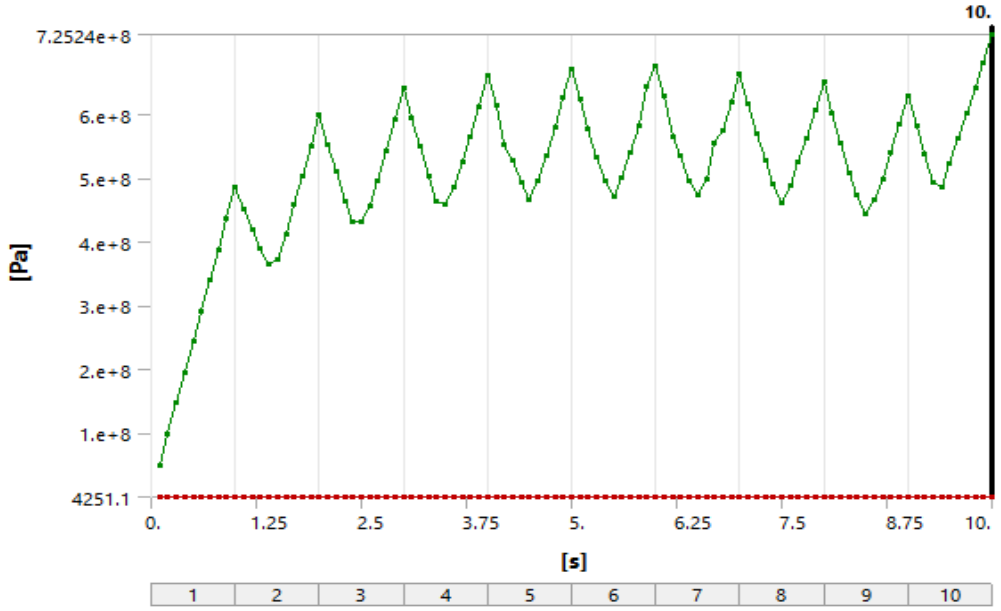

Fig. 19: Variation of Von-Mises Stresses during the laser cutting process (for sample 'O',i.e. age hardening time is 5Hr)

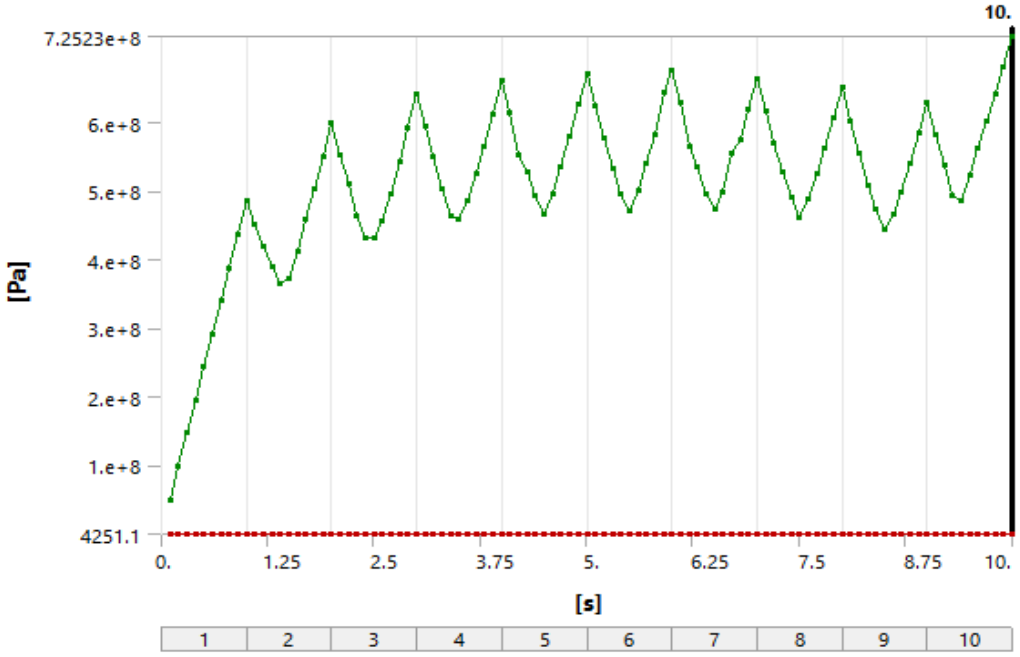

Fig. 20: Variation of Von-Mises Stresses during the laser cutting process (for sample 'W',i.e. age hardening time is 10Hr)

Figure 19 and 20 represents the variation of Von-Mises stresses of Al 7075 T6 workpiece during laser cutting process. It also indicates that stress values are gradually increases up to 6 sec and then

slightly decreases up to 9 sec. After 9 secs, again it is increasing and becomes maximum value at 10 sec.

4.3 Mechanical Test for Tensile properties

Tensile testing of all these specimens was conducted as per IS 1608 : 2005 with circular cross-section test pieces. Two samples were tested from each heat-treated condition and as cast samples (as shown in Fig. 21). The tests were carried out at room temperature with a crosshead speed of 1 mm/min using a computerized UTES-60 universal testing machine (as shown in Fig. 22) . General Specification of UTM Machine are given in Table 5. Load – displacement plots were obtained on an X-Y recorder and ultimate tensile strength and percentage elongation values were calculated from this load – displacement diagrams. The average values from three test samples are reported here.

Fig. 21: Circular cross-section test pieces

Table 5 : General Specification Of UTM Machine

Parameters	Value
Maximum Capacity	600
Measuring range	0-600
Load resolution (20000 counts full scale)	30
Load range with accuracy of Measurement +/-1%	12 to 600
Resolution of piston movement (Displacement)	0.01
Clearance for tensile test (At fully descended working piston)	50-800
Clearance for compression test (At fully descended working piston)	0-800
Ram Stroke	250
Straining/ Piston Speed (at no load)	0-100

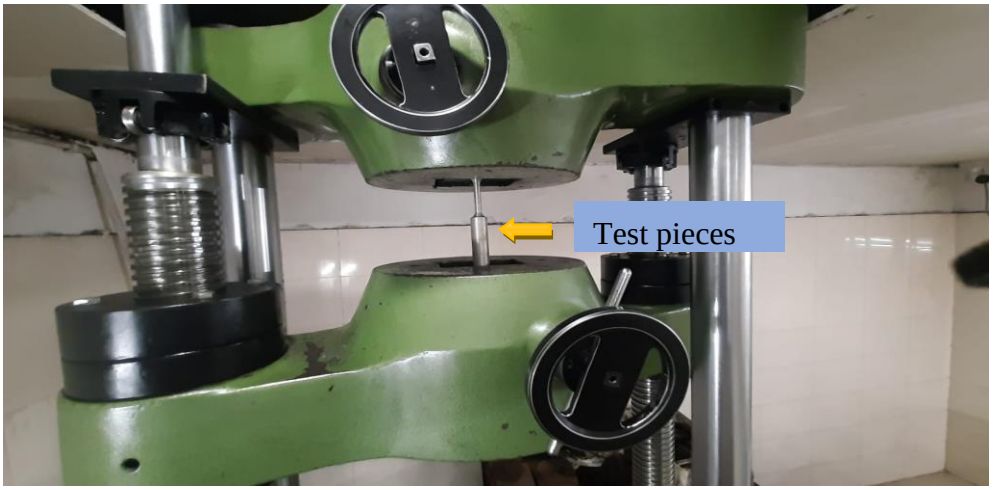

Fig. 22: UTM Machine

The specimen U at a temperature 480°C for 1 hours followed by rapid quenching in ice cool water. These quenched samples were then subjected to a precipitation hardening treatment (age hardening) by heating them to 120°C , holding them at this temperature for 5 hours and then followed by air cooling to room temperature. The sample U dimensions for the tensile test are given in table 6. The

results after the tensile test for the sample U are represented in table 7. The displacement vs load plot generated from the tensile test for the sample U are portrayed in Fig. 23. It shows that load is gradually increases up to displacement 13.32 mm and it reaches maximum value of load is 47.5 kN. Fractured test Sample U after breaking during tensile test is shown in the Fig. 24.

Table 6 : Input Data in UTM Machine for Sample U

Parameters	**Value**
Gauge Length (mm)	50.0
Outer Diameter (mm)	10.0
Initial Area (mm)	78.54
Final Diameter (mm)	9.34

Table 7 : Material Test Result of Sample U

Parameters	**Value**
Max. Load (kN)	47.5
Ult. Stress (kN/mm^2)	0.61
Disp. At Max. Load (mm)	13.32
Max. Displacement (mm)	13.56
Yield Load (kN)	44.196
Yield Stress (kN/mm^2)	0.563
YS/UTS	0.922
UTS/YS	1.058
Final CS. Area (mm^2)	68.51
Reduction in Area %	12.771
Final Gauge Length (mm)	54.92
Elongation %	9.840

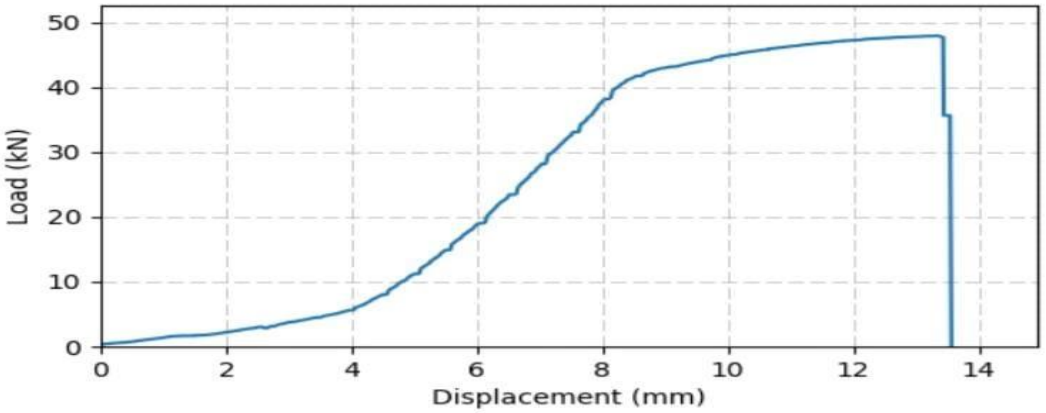

Fig. 23: Graph Displacement Vs Load (Sample U) 5 Hours

Fig. 24: Fractured test for Sample U after breaking during tensile test

The specimen W at a temperature 480°C for 1 hours followed by rapid quenching in ice cool water .These quenched samples were then subjected to a precipitation hardening treatment (age hardening) by heating them to 120°C , holding them at this temperature for 10 hours and then followed by air cooling to room temperature.

The sample W dimensions for the tensile test are given in Table 8. The results after the tensile test for the sample W are represented in Table 9. The displacement vs load plot generated from the tensile test for the sample W are portrayed in Fig. 25. It shows that load is gradually increases up to displacement 11.09 mm and it reaches maximum value of load is 49.5 kN Fractured test Sample W after breaking during tensile test is shown in the Fig. 26.

Table 8 : Input Data in UTM Machine for Sample W

Parameters	**Value**
Gauge Length (mm)	50.0
Outer Diameter (mm)	10.0
Initial Area (mm)	78.54
Final Diameter (mm)	9.35

Table 9 : Material Test Result of Sample W

Parameters	**Value**
Max. Load (kN)	49.5
Ult. Stress (kN/mm^2)	0.63
Disp. At Max. Load (mm)	11.09
Max. Displacement (mm)	11.3
Yield Load (kN)	46.992
Yield Stress (kN/mm^2)	0.598
YS/UTS	0.949
UTS/YS	1.053
Final CS. Area (mm^2)	68.66
Reduction in Area %	12.580
Final Gauge Length (mm)	53.08
Elongation %	6.160

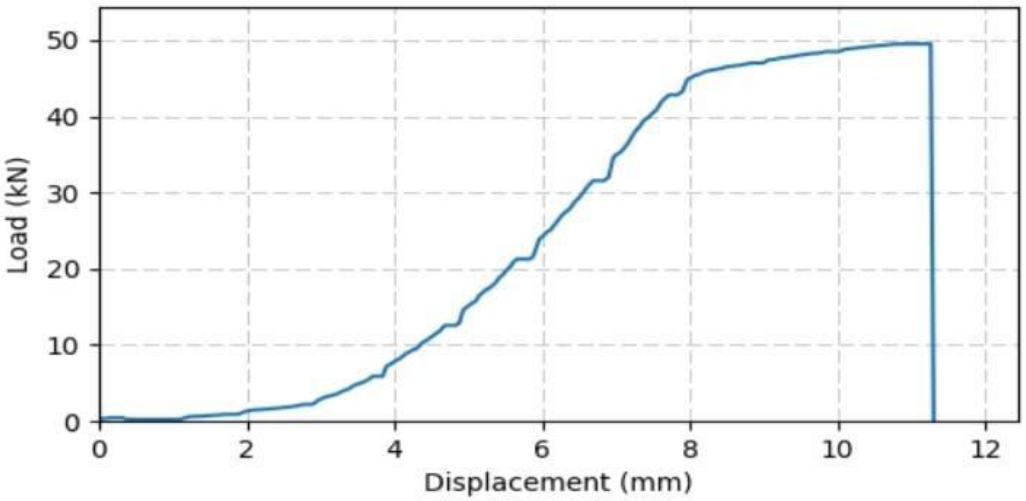

Fig. 25: Graph Displacement Vs Load (Sample W) 10 Hours

Fig. 26: Fractured test Sample W after breaking during tensile test

4.4 Mechanical Test for hardness properties

4.4.1 Rockwell Hardness Test

The Rockwell hardness are measured in the Rockwell Hardness Machine as specified in the Table 10. ISO 6508-1 Part 1 standard is followed for the Rockwell hardness test measurement. Fig 27 (a) represents the Rockwell Hardness Test Machine along with Sample W while the Fig 27 (b) shows the spot/indentation after hardness measurement. The control and the heat-treated samples are

subjected to the Rockwell hardness test using Rockwell B hardness scale (HRB) and the result shown in Table 11. From the results of hardness test, sample W has the highest average hardness value followed by sample A. Sample A, sample E, sample I, Sample O, Sample U and sample W. The results of the hardness test were proportional to the microstructure morphology. The growing precipitate due to aging will affect the hardness value of aluminum.

The phenomenon of increasing mechanical properties, in this case the hardness of aluminum alloy which have been done an aging process, occurs because the formation of precipitates often leads to the formation of dislocations in the crystal lattice of the solvent atom. Dislocations can be formed if the atomic size of the precipitate is different from the size of the atom of the solvent, if the size of the precipitate is smaller, it will cause tensile stress, and if the size is greater, the precipitate particles will cause compressive stress, the dislocation will also cause a force field. Dislocation will be like being drawn towards the precipitate. Sample Kept for 1h at 480°C, the average HRB value is 54.

Table 10 : Rockwell Hardness Machine Specification

Parameters	**Value**
Scale	B
Indentor	1.588 mm 1/16 in Ball
Total Force	100 kgf
Preliminary Force	98.07 kgf

Table 11 : Rockwell Hardness Test Chart B Scale (HRB)

	Sample ID					
Spot	A	E	I	O	U	W
1	70	75	78	83	83	89
2	73	77	75	82	84	86.5
3	77	76	77	83	83	89
4	79	73	79	82	85	88
Average	74.5	75.25	77.25	82.5	83.75	88.12

(a) (b)

Fig. 27: (a) Rockwell Hardness Test Machine With Sample (W), (b) Hardness Testing Spot of HRB

4.4.2 Brinell Hardness Test

The Brinell Hardness are measured in the Brinell Hardness Machine as specified in the Table 12. ISO 6506 standard is followed for the Brinell hardness test measurement. Fig 28 shows the spot/indentation after hardness measurement. The control and the heat-treated samples are subjected to the Brinell hardness test and the results for each sample are shown in Table 13. From the results of hardness test, sample W has the highest average hardness value followed by sample U, sample O, sample A, Sample I, and sample E.

Table 12 : Brinell Hardness Machine Specification

Parameters	**Value**
Test Force	3000 Kg/mm^2
Indenter Dia	10 mm
Indenter Type	Hard Metal Ball

Table 13 : Brinell Hardness Test (BHN)

Spot	Sample ID					
	A	E	I	O	U	W
1	156	148	149	157	162	170
2	155	149	151	159	165	169
3	157	150	152	158	161	171
4	156	149	151	159	163	170
Average	156	149	150.75	158.25	162.75	170

Fig. 28: Hardness Testing Spot (BHN)

4.4.3 Micro Vickers Hardness Test

The Micro Vickers Hardness are measured in the Micro Vickers Hardness Machine as specified in the Table 14. ASTM E384 standard is followed for the Micro Vickers hardness test measurement. Figure 29 shows the Micro Vickers Hardness Machine where the sample are kept for measurement. 1 Kg load is applied while three different holding time i.e 10sec, 20sec and 30 secs are used to measure the hardness. The results of the Micro Vickers hardness for different samples are shown in Table 15. From the results of hardness test, sample W has the highest average hardness value followed by sample U, sample O, sample A, sample I and sample E. Figure 30 represents the Micro Vickers Hardness Graph with different holding time. Holding Time 10 sec predicts higher Vickers hardness for aging time 15min, 60 min, 120 min while for aging time 30min and 300 min VHN invariant with holding time.

Table 14 : Machine Specification Of Micro Vickers (FMV – 1)

Parameters	**Value**
Maximum Test Height	115mm
Throat of Machine	70mm
Test Load	10,25,50,100 gms. & 200 to 1000 gms
Load Accuracy	A+_1% of nomilal load value
Type of Indentor	Micro Vickers Diamond Indenter (136 Â° Pyramid)
Objective Magnification	10X,20X, and 50X selectable
Eyepiece Magnification	12.5X (Approx)
Total Magnification	125X, 250X and 625X
Max.Diagonal Measurment (Field of View)	10X Objective – 1mm 20X Objective – 0.5mm 50X Objective – 0.2mm
Size of table top	100 mm x 100 mm
Max . travel XX & YY axis	50 mm each
Least count of Measurment	0.01 mm
Application of Test load	By a two position hand operated lever
Remove of test load	Automatic
Power	50 Watts

Table 15 : Micro Vickers Hardness Tester (FMV – 1)

Mark	Hardness value in Micro Vickers at 1 Kg load		
	1 Kg/10 Sec	1 Kg/20 Sec	1 Kg/30 Sec
A	151 HV1	143 HV1	145 HV1
E	135 HV1	135 HV1	135 HV1
I	148 HV1	148 HV1	143 HV1
O	168 HV1	165 HV1	165 HV1
U	168 HV1	168 HV1	168 HV1
W	168 HV1	171 HV1	171 HV1
Average Value	156.33 HV1	155 HV1	154.5 HV1

Fig. 29: Micro Vickers Hardness Machine with the sample for measurement of Hardness

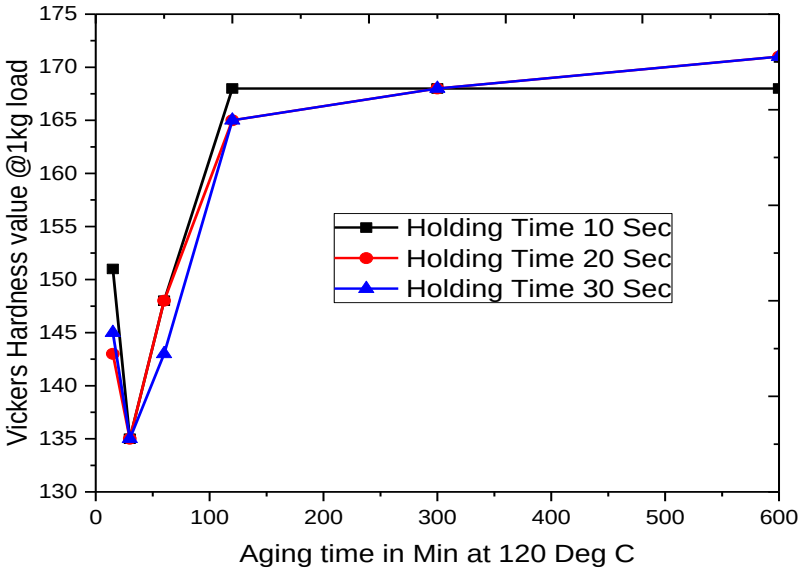

Fig. 30: Micro Vickers Hardness Graph with different holding time

Chapter 5

Microscopic study

5.1 Microstructure analysis

Samples of 7075-T6 Al alloy which have been etched will be seen in the microstructure using an optical microscopy with 200x magnification. The specimen surface must first be ground and polished to a smooth and mirror like finish. This is accomplished by using successively finer abrasive papers and powders (as shown in Fig.31). Polishing with water and micro structure view are shown in the Fig.32 and Fig.33, respectively. Fig 34 presents the image of Electron Microscope (APOLLO). Fig. 35, 36, 37, 38, 39, and 40 shows the microstructure of the sample A, sample E, sample I, sample O, sample U and sample W respectively. The general specifications of the microscope are given in the table 16 while the Electron Microscope Specification (Apollo) is shown in table 17. The results of the five microstructure drawings are almost similar, where it shows the finely dispersed precipitate of η'-$MgZn_2$ and η-$MgZn_2$ in aluminum matrix. From the results of the optical metallography there are differences in the microstructure, the farther sample from the furnace door, the more precipitates in the Al phase formed. The microstructure consists of elongated and fibroid grains with some dispersed particles, indicating the alloy has not recrystallized even after T6 heat treatment. Fine precipitates were evident in original grain interiors and in subgrain boundaries. It can be seen that the number of precipitates formed is not as much as in . However, sample E was over etched due to the immersion time about 60 s. Over Etching does not really affect the observation, just a little difficult to identify the microstructure.

Table 16 : General specifications of the microscope

Parameters	Value
Type of Microscope	Stereo microscope, Greenough design
Design Principle	Two zoom systems, tilted by the stereo angle
Stereoscopic View	Three dimensional observation through eyepieces
Apochromatic Corrected Zoom and Front Optics	Image free of color fringes in complete magnification range
Manual Zoom, Zoom Range	8:1 (0.63×...5.0×)
Quality of Zoom Optics	Distortion free, excellent contrast, apochromatic corrected
Ergonomic Viewing Angle	35°
Adjustment of Interocular Distance	55 – 75 mm
Eyepieces	d = 30 mm
Stemi Mounts	d = 76 mm
Illuminators	d = 53 mm; Illuminators d = 66 mm via clamp ring d53/66
Working Surface	W255 × D215 mm
Height / Lifting range	360 mm / 190 mm
Load capacity of Stemi mount	5 kg

Grit	Abrasive Grain Microns
400	25
600	15
800	10
1000	5
1200	3

Fig. 31: Polishing Paper Silicon Carbide Waterproof

Fig. 32: Polishing With Water

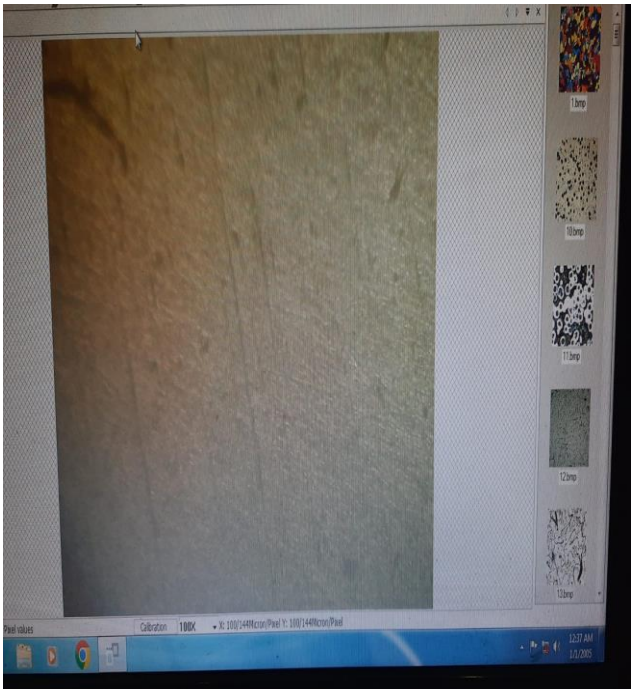

Fig. 33: Micro Structure View

Table 17 : Electron Microscope Specification (Apollo)

Parameters	**Value**
Zoom	Mono zoom variable magnification system
Zoom Ratio	10:1 (0.63 X – 6.3 X)
Aperture Iris Diaphragm	Built - in
Illumination Mode	Coaxial reflected light
Light Path Selection	2 step binocular 100%, photo 100%
Tilting Angle	0° – 23° continuously

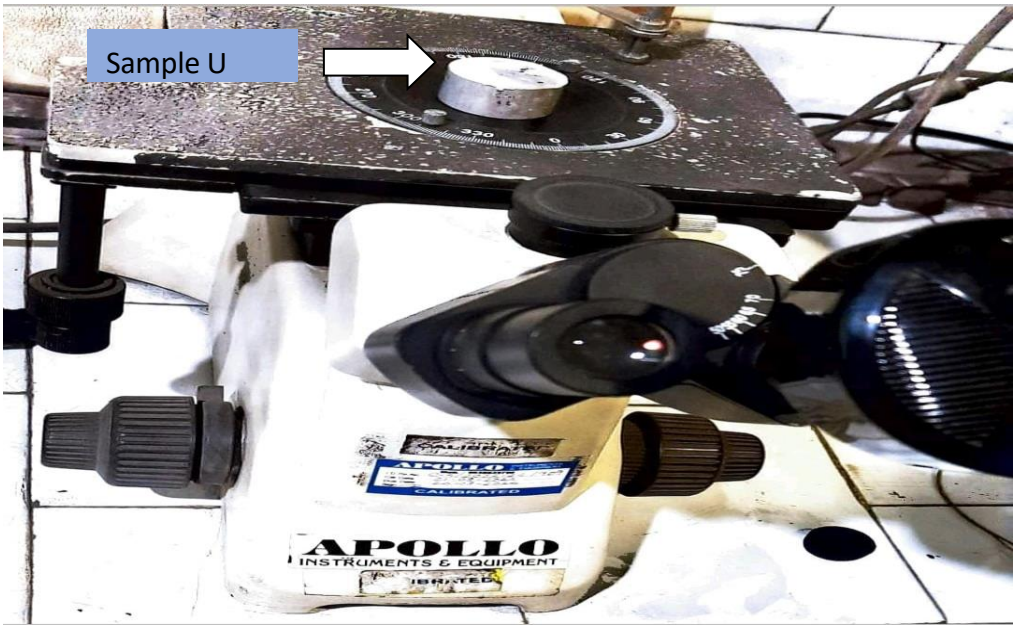

Fig. 34: Electron Microscope (APOLLO)

Sample ‘A’ kept for 1h at 480°C, thereafter aging time 15 min at 120°C. As per micro structure test report, the grain size of the sample ‘A’ is 6 as shown in Fig. 35.

Fig. 35: Micro Structure Test Report of Sample ‘A’

Sample ‘E’ kept for 1h at 480°C, thereafter aging time 30 min at 120°C. As per micro structure test report, the Grain Size of the sample ‘E’ is 5 as shown in Fig. 36.

Fig. 36: Micro Structure Test Report of Sample ‘E’

Sample ‘I’ kept for 1h at 480°C, thereafter aging time 60 min at 120°C. As per micro structure test report, the grain size of the sample ‘I’ is 6 as shown in Fig. 37.

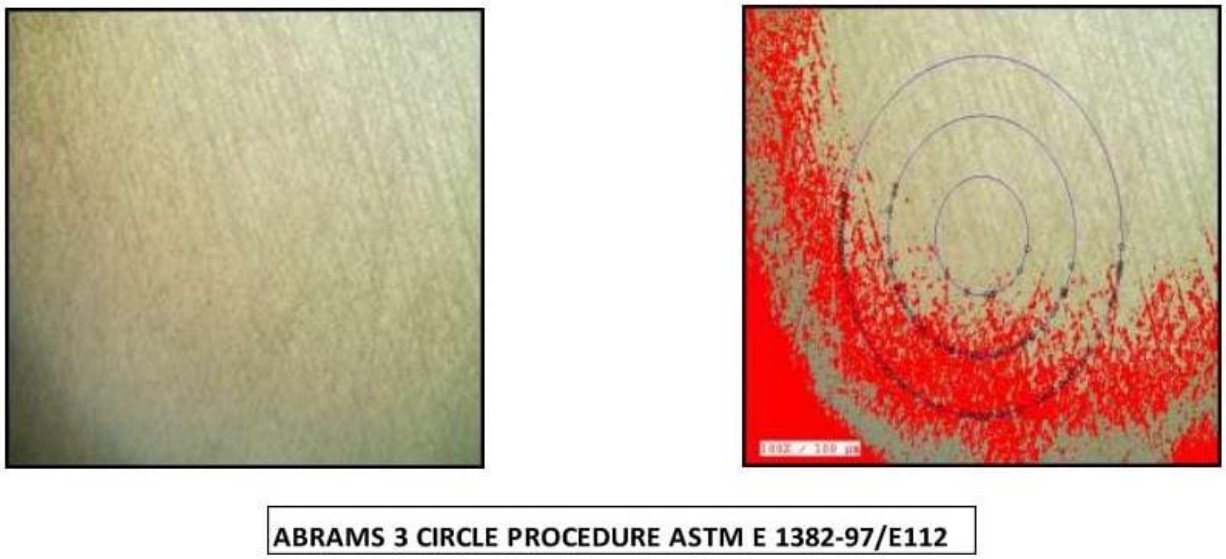

Fig. 37: Micro Structure Test Report of Sample ‘I’

Sample ‘O’ kept for 1h at 480°C, thereafter aging time 120 min at 120°C. As per micro structure test report, the grain size of the sample ‘O’ is 6 as shown in Fig. 38.

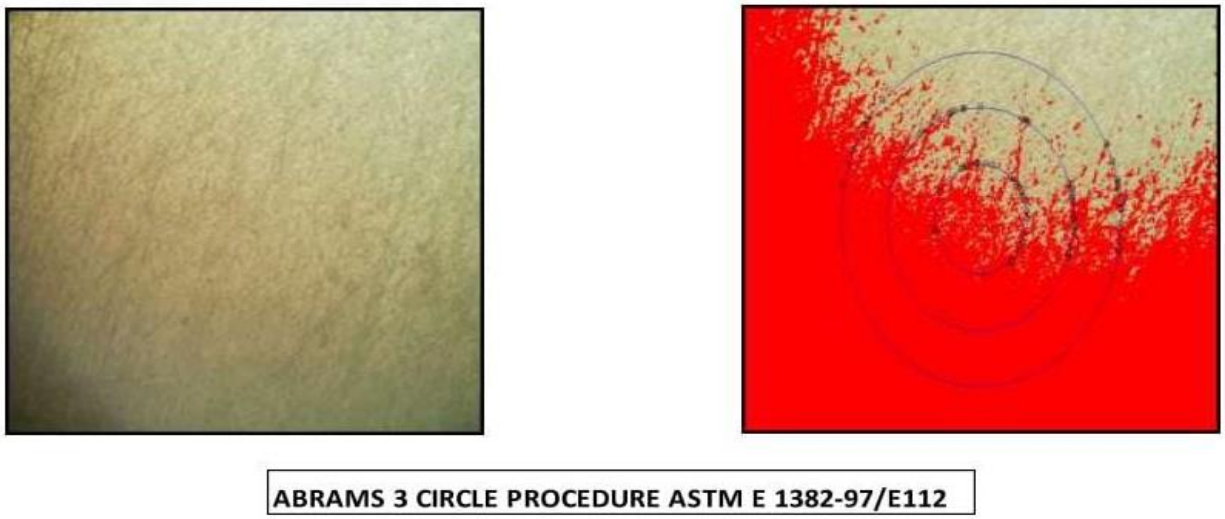

Fig. 38: Micro Structure Test Report of Sample ‘O’

Sample ‘U’ Kept for 1 h at 480°C, thereafter aging time 300 min at 120°C. As per micro structure test report, the grain size of the sample ‘U’ is 6 as shown in Fig. 39.

Fig. 39: Micro Structure Test Report of Sample ‘U’

Sample ‘W’ kept for 1h at 480°C, thereafter aging time 600 min at 120°C. As per micro structure test report, the grain size of the sample ‘W’ is 6 as shown in Fig. 40.

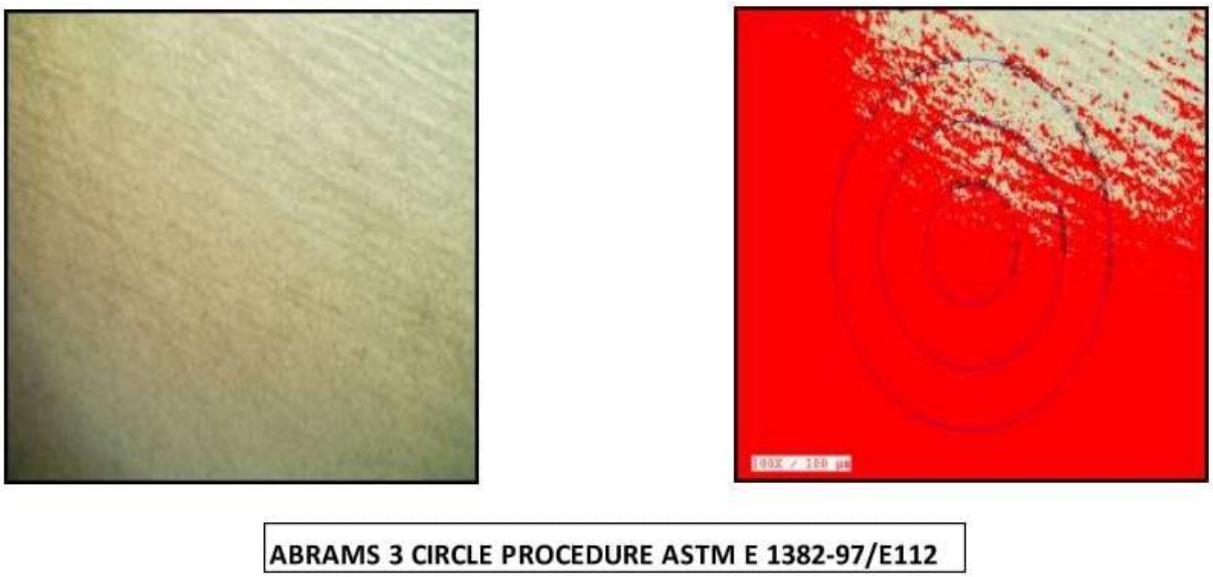

Fig. 40: Micro Structure Test Report of Sample ‘W’

Chapter 6

Conclusions and Future Scope

6.1 Conclusions

In this work modeling of the laser cutting of Al 7075 T6 alloy and the thermal treatment of the Al 7075 T6 alloy at different aging temperature and holding time are performed. Stress distribution and HAZ for the laser cutting are evaluated. The hardness of the 7075 Alloy samples for different aging temperature and holding time are evaluated. Based on the present work the following conclusions can be drawn.

a) The high thermal conductivity of the aluminum alloy is considered to be the reason for the apparent increase in temperature behind the laser beam spot along the surface during the cutting process.

b) Scanning line of the work piece surface where they affected by the focused laser beam achieved high values of von Mises stress. It can be concluded from the figures that maximum Von-Mises stress is observed for sample 'O' with aging time 120 min.

c) Al 7075 Alloy sample are prepared for 1h at 480°C heat treated following different aging time 15min, 30 min, 60 min, 120 min, 300 min, 600 min at 120°C

d) The Rockwell Hardness in B scale is measured. HRB values are observed to increase with the aging time. HRB 89 is observed with aging time 600 min at 120°C.

e) HRB values increases 64% with aging time 600 min compared to without aging case. Even 15 min aging time increases the HRB value by 46%.

f) For Micro Vickers Hardness Test aging time 120 min produces satisfactory hardness value.

g) From the tensile test it was observed that Ultimate stress reaches to 610 Mpa.

h) Aluminum 7075 needs thermal treatment for high-strength applications where improved surface hardness and ultimate strength can be achieved. Aging time 120 min produces satisfactory surface hardness compared to without aging case.

6.2 Future Scope of Work

The following future research directions can be explored for further carry forward the present work

a) The thermal fatigue analysis due to the laser cutting can be explored.

b) Laser cladding on the Al 5075 Alloy can be performed for repair and maintenance of the damaged or worn out components of this grade alloy.

c) This study can be extended to the other Al alloy for suitable application in aerospace energy field.

d) Welding of dissimilar al alloy can be explored using Laser technique or other welding technique.

References

[1] Kim SW, Kim DY, Kim WG, Woo KD. The study on characteristics of heat treatment of the direct squeeze cast 7075 wrought Al alloy. Materials Science and Engineering: A. 2001 May 31;304:721-6.

[2] Dong J, Cui JZ, Le QC, Lu GM. Liquidus semi-continuous casting, reheating and thixoforming of a wrought aluminum alloy 7075. Materials Science and Engineering: A. 2003 Mar 25;345(1-2):234-42.

[3] Liu D, Atkinson HV, Kapranos P, Jirattiticharoean W, Jones H. Microstructural evolution and tensile mechanical properties of thixoformed high performance aluminium alloys. Materials Science and Engineering: A. 2003 Nov 25;361(1-2):213-24.

[4] Chayong S, Atkinson HV, Kapranos P. Thixoforming 7075 aluminium alloys. Materials Science and Engineering: A. 2005 Jan 15;390(1-2):3-12.

[5] Clark Jr R, Coughran B, Traina I, Hernandez A, Scheck T, Etuk C, Peters J, Lee EW, Ogren J, Es-Said OS. On the correlation of mechanical and physical properties of 7075-T6 Al alloy. Engineering Failure Analysis. 2005 Aug 1;12(4):520-6.

[6] Es-Said OS, Ruperto TM, Vasquez SL, Yue AY, Manriquez DJ, Quilla JC, Harris SH, Hannan S, Foyos J, Lee EW, Pregger B. Warpage behavior of 7075 aluminum alloy extrusions. Journal of Materials Engineering and Performance. 2007 Apr;16:242-7.

[7] Kim SK, Yoon YY, Jo HH. Novel thixoextrusion process for Al wrought alloys. Journal of materials processing technology. 2007 Jun 12;187:354-7.

[8] Turkmen HS, Loge RE, Dawson PR, Miller MP. On the mechanical behaviour of AA 7075-T6 during cyclic loading. International Journal of fatigue. 2003 Apr 1;25(4):267-81.

[9] Jabra J, Romios M, Lai J, Lee E, Setiawan M, Ogren JR, Clark R, Oppenheim T, Es-Said OS, Lee EW, Abourialy N. The effect of thermal exposure on the mechanical properties of 2099-T6 die forgings, 2099-T83 extrusions, 7075-T7651 plate, 7085-T7452 die forgings, 7085-T7651 plate, and 2397-T87 plate aluminum alloys. Journal of materials engineering and performance. 2006 Oct;15:601-7.

[10] Emani SV, Benedyk J, Nash P, Chen D. Double aging and thermomechanical heat treatment of AA7075 aluminum alloy extrusions. Journal of materials science. 2009 Dec;44:6384-91.

[11] Li JF, Peng ZW, Li CX, Jia ZQ, Chen WJ, Zheng ZQ. Mechanical properties, corrosion behaviors and microstructures of 7075 aluminium alloy with various aging treatments.

Transactions of Nonferrous Metals Society of China. 2008 Aug 1;18(4):755-62.

[12] Wannasin J, Janudom S, Rattanochaikul T, Canyook R, Burapa R, Chucheep T, Thanabumrungkul S. Research and development of gas induced semi-solid process for industrial applications. Transactions of Nonferrous Metals Society of China. 2010 Sep 1;20:s1010-5.

[13] Mächler R, Uggowitzer PJ, Solenthaler C, Pedrazzoli RM, Speidel MO. Structure, mechanical properties, and stress corrosion behaviour of high strength spray deposited 7000 series aluminium alloy. Materials Science and Technology. 1991 May;7(5):447-51.

[14] Tan CF, Radzai SM. Effect of hardness test on precipitation hardening aluminium alloy 6061-T6. Chiang Mai Journal of Science. 2009;36(3):276-86.

[15] Isadare AD, Aremo B, Adeoye MO, Olawale OJ, Shittu MD. Effect of heat treatment on some mechanical properties of 7075 aluminium alloy. Materials Research. 2013;16:190-4.

[16] Staley JT. Proc. 3rd Int. Conf. on Al. Alloys (eds. L. Arnberg, O. Lohne, E. Nes, N. Ryum), p.107, Norwegian Institute of Technology, SINTEF, Trondheim, Norway (1992).

[17] Du ZW, Sun ZM, Shao BL, Zhou TT, Chen CQ. Quantitative evaluation of precipitates in an Al–Zn–Mg–Cu alloy after isothermal aging. Materials Characterization. 2006 Mar 1;56(2):121-8.

[18] ASM International Handbook Committee, American Society for Metals. Heat Treating Division. Heat treating. ASM international; 1991.

[19] Mahathaninwong N, Plookphol T, Wannasin J, Wisutmethangoon S. T6 heat treatment of rheocasting 7075 Al alloy. Materials Science and Engineering: A. 2012 Jan 15;532:91-9.

[20] Padap AK, Yadav AP, Kumar P, Kumar N. Effect of aging heat treatment and uniaxial compression on thermal behavior of 7075 aluminum alloy. Materials Today: Proceedings. 2020 Jan 1;33:5442-7.

[21] Thanabumrungkul S, Janudom S, Burapa R, Dulyapraphant P, Wannasin J. Industrial development of gas induced semi-solid process. Transactions of Nonferrous Metals Society of China. 2010 Sep 1;20:s1016-21.

[22] Spencer DB, Mehrabian R, Flemings MC. Rheological behavior of Sn-15 pct Pb in the crystallization range. Metallurgical and Materials Transactions B. 1972 Jul;3:1925-32.

[23] Atkinson HV. Modelling the semisolid processing of metallic alloys. Progress in materials science. 2005 Mar 1;50(3):341-412.

[24] Curle UA, Govender G. Semi-solid rheocasting of grain refined aluminum alloy 7075. Transactions of Nonferrous Metals Society of China. 2010 Sep 1;20:s832-6.

[25] Song M, Chen K. Effects of the enhanced heat treatment on the mechanical properties and

stress corrosion behavior of an Al–Zn–Mg alloy. Journal of materials science. 2008 Aug;43(15):5265-73.

[26] Mukhopadhyay AK. Microstructure and properties of high strength aluminium alloys for structural applications. Transactions of the Indian Institute of Metals. 2009 Apr;62:113-22.

[27] Ince JC, Peerzada M, Mathews LD, Pai AR, Al-Qatatsheh A, Abbasi S, Yin Y, Hameed N, Duffy AR, Lau AK, Salim NV. Overview of emerging hybrid and composite materials for space applications. Advanced Composites and Hybrid Materials. 2023 Aug;6(4):130.

[28] Sánchez-Roncero A, Garibo-i-Orts Ò, Conejero JA, Eivazi H, Mallor F, Rosenberg E, Fuso-Nerini F, García-Martínez J, Vinuesa R, Hoyas S. The sustainable development goals and aerospace engineering: a critical note through artificial intelligence. Results in Engineering. 2023 Mar 1;17:100940.

[29] Sadhu KK, Mandal N, Sahoo RR. SiC/graphene reinforced aluminum metal matrix composites prepared by powder metallurgy: A review. Journal of Manufacturing Processes. 2023 Apr 7;91:10-43.

[30] Garg P, Jamwal A, Kumar D, Sadasivuni KK, Hussain CM, Gupta P. Advance research progresses in aluminium matrix composites: manufacturing & applications. Journal of materials research and technology. 2019 Sep 1;8(5):4924-39.

[31] Senthil S, Raguraman M, Manalan DT. Manufacturing processes & recent applications of aluminium metal matrix composite materials: A review. Materials Today: Proceedings. 2021 Jan 1;45:5934-8.

[32] McMullen P. Fibre/resin composites for aircraft primary structures: a short history, 1936–1984. Composites. 1984 Jul 1;15(3):222-30.

[33] Lu K. The future of metals. Science. 2010 Apr 16;328(5976):319-20.

[34] Khalid MY, Al Rashid A, Sheikh MF. Effect of anodizing process on inter laminar shear strength of GLARE composite through T-peel test: experimental and numerical approach. Experimental Techniques. 2021 Apr;45(2):227-35.

[35] Findlay SJ, Harrison ND. Why aircraft fail. Materials today. 2002 Nov 1;5(11):18-25.

[36] Breuer UP. Commercial aircraft composite technology. Cham: Springer International Publishing; 2016 May 10.

[37] Luo K, Xiong H, Zhang Y, Gu H, Li Z, Kong C, Yu H. AA1050 metal matrix composites reinforced by high-entropy alloy particles via stir casting and subsequent rolling. Journal of Alloys and Compounds. 2022 Feb 10;893:162370.

[38] Idusuyi N, Olayinka JI. Dry sliding wear characteristics of aluminium metal matrix composites: a brief overview. Journal of Materials Research and Technology. 2019 May

1;8(3):3338-46.

[39] E. Kannatey-Asibu Jr., Principles of Laser Materials Processing, first ed., John Wiley & Sons Inc., New Jersy, 2009.

[40] Araujo D, Carpio FJ, Mendez D, Garcıa AJ, Villar MP, Garcıa R, Jimenez D, Rubio L. Microstructural study of CO2 laser machined heat affected zone of 2024 aluminum alloy. Applied surface science. 2003 Mar 15;208:210-7.

[41] Stournaras A, Stavropoulos P, Salonitis K, Chryssolouris G. An investigation of quality in CO2 laser cutting of aluminum. CIRP Journal of Manufacturing Science and Technology. 2009 Jan 1;2(1):61-9.

[42] Dubey AK, Yadava V. Optimization of kerf quality during pulsed laser cutting of aluminium alloy sheet. Journal of materials processing technology. 2008 Aug 11;204(1-3):412-8.

[43] Sharma A, Yadava V. Modelling and optimization of cut quality during pulsed Nd: YAG laser cutting of thin Al-alloy sheet for curved profile. Optics and Lasers in Engineering. 2013 Jan 1;51(1):77-88.

[44] Riveiro A, Quintero F, Lusquiños F, Comesaña R, Pou J. Parametric investigation of CO2 laser cutting of 2024-T3 alloy. Journal of Materials Processing Technology. 2010 Jun 19;210(9):1138-52.

[45] Kardas OO, Keles O, Akhtar S, Yilbas BS. Laser cutting of rectangular geometry in 2024 aluminum alloy: Thermal stress analysis. Optics & Laser Technology. 2014 Dec 1;64:247-56.

[46] Yilbas BS, Akhtar SS, Keles O, Boran K. Laser cutting of triangular geometry into 2024 aluminum alloy: Influence of triangle size on thermal stress field. Journal of Mechanical Science and Technology. 2015 Aug;29:3239-48.

[47] Yilbas BS, Akhtar SS, Keles O. Laser cutting of triangular geometries in aluminum foam: Effect of cut size on thermal stress levels. Optics & Laser Technology. 2013 Jun 1;48:523-9..

[48] Leone C, Genna SI, Caggiano AL, Tagliaferri VI, Molitierno R. An investigation on Nd: YAG laser cutting of Al 6061 T6 alloy sheet. Procedia Cirp. 2015 Jan 1;28:64-9.

[49] Sharma A, Yadava V. Modelling and optimization of cut quality during pulsed Nd: YAG laser cutting of thin Al-alloy sheet for straight profile. Optics & Laser Technology. 2012 Feb 1;44(1):159-68.

[50] Bahoter, N.B.; and Harimkar, S.P. (2008). laser fabrication and machining of materials. Springer, New York.

[51] Sharma, P.; Dubey, A.K.; and Pandey, A.K. (2014). Numerical study of temperature and stress fields in laser cutting of aluminum alloy sheet. International conference on advance in manufacturing and material engineering, 5(2), 1887 – 1896.

[52] Sowdari, D.; and Majumdar, P. (2010). Finite element analysis of laser irradiation metal heat and melting process. Optics and laser technology, 42(6), 855-865.